The Thesis committee for Yuyang Wang

Certifies that this is the approved version of the following thesis

MmWave vehicle-to-infrastructure communication: Analysis of urban microcellular networks

APPROVED BY

SUPERVISING COMMITTEE:

Robert W. Heath, Jr., Supervisor

Gustavo de Veciana

MmWave vehicle-to-infrastructure communication: Analysis of urban microcellular networks

by

Yuyang Wang , B.S.

THESIS

Presented to the Faculty of the Graduate School of

The University of Texas at Austin

in Partial Fulfillment

of the Requirements

for the Degree of

MASTER OF SCIENCE IN ENGINEERING

THE UNIVERSITY OF TEXAS AT AUSTIN

May 2017

Dedicated to my parents, Xingtang Wang and Yanfang Wei

Acknowledgments

I would like to start by thanking my parents for their support through my almost twenty-year education in school and their unconditional love and patience. Their love and support guide me through life and make me myself. Then, I would like to express my sincere gratitude for my supervisor Prof. Robert W. Heath Jr.. His broad knowledge and sharp insights on our research area provide me with numerous motivations throughout the pursuit of my master degree. I would also like to thank him for his patience for me as a new student and his heart-warming concern when I was having a hard time. I am also very grateful to my committee member and also my course lecturer Prof. Gustavo de Veciana for his expertise in my research area and his fantastic teaching style, and more importantly, his valuable comments and instructions on my work, which help improve the thesis a lot. I would like to thank my mentor Dr. Kiran Venugopal for his help and instructions during my two years' study and research, and Prof. Andreas F. Molisch for his collaboration and instructions that lead to the accomplishment of this work. I would also like to thank my dear friend, Yixuan Zhang, for her almost one-decade accompany as the best friend forever.

Lastly, I would like to mourn the loss of the life of a precious young man, Harrison Brown, in an accidental tragedy on UT campus, May 1st, 2017.

The peace and kindness of human nature should always be treasured.

MmWave vehicle-to-infrastructure communication: Analysis of urban microcellular networks

by

Yuyang Wang , MS.E.
The University of Texas at Austin, 2017

Supervisor: Robert W. Heath, Jr.

Vehicle-to-infrastructure (V2I) communication may provide high data rates to vehicles via millimeter-wave (mmWave) microcellular networks. This thesis uses stochastic geometry to analyze the coverage of urban mmWave microcellular networks. Prior work used a pathloss model with a line-of-sight probability function based on randomly oriented buildings, to determine whether a link was line-of-sight or non-line-of-sight. In this thesis, we use a pathloss model inspired by measurements, which uses a Manhattan distance model and accounts for differences in pathloss exponents and losses when turning corners. In our model, streets and base stations (BSs) are randomly located on a network formed by a two dimensional Poisson line process. Our model is well suited for urban microcellular networks where the base stations are deployed at street level. Based on this new approach, we derive the coverage probability under certain BS association rules to obtain closed-form solutions without much complexity. In addition, we draw two main conclusions from our

work. First, non-line-of-sight BSs are not a major benefit for association or source of interference. Second, there is an ultra-dense regime where deploying (active) BSs does not enhance coverage.

Table of Contents

List of Tables

List of Figures

Chapter 1

Introduction

Vehicle-to-infrastructure (V2I) communication offers the potential to enhance safety and efficiency in urban vehicular networks [1–3]. Combined with millimeter wave (mmWave) [4–6], V2I has the potential to offer high data rates and low latency [7–9], to enable massive data sharing among a great number and diversity of mobile devices in vehicular networks [7, 10]. MmWave communication not only has access to larger bandwidths, it can also allow compact yet very large antenna arrays at both the transmitter and receiver to provide high directional beamforming gains and low interference. Compared to channels at microwave frequencies (<6 GHz), however, mmWave channels are more sensitive to blockage losses, especially in the urban streets where signals are blocked by high buildings, vehicles or pedestrians [9], [11], and sharp transitions from line-of-sight (LOS) to non-line-of-sight (NLOS) links are more common[1]. This motivates the study of mmWave microcellular network performance in the context of vehicular urban areas.

[1]In the current thesis, LOS is defined as "optical" line of sight between the transmitter and receiver *location* as the papers cited here. NLOS happens when the link between the transmitter and the receiver is blocked by obstructions, specifically in our thesis, is blocked by urban buildings.

Stochastic geometry Stochastic geometry has been used extensively to analyze performance in mmWave cellular networks [12–17]. BS and cellular user locations are modeled as Poisson point processes on a two-dimensional plane, based on which the coverage probablity of a *typical* cellular user is derived. Also, building blockages are considered as the main source differentiating LOS and NLOS links, with a few papers analyzing different building blockage models. Unfortunately, prior work analyzing mmWave cellular networks in [12–17] employed a pathloss model with a LOS probability function based on Euclidean distance [18], to determine whether a link was LOS or NLOS. This works well for randomly oriented buildings [13], but does not properly model V2I networks where strong LOS interference may result from infrastructure co-located on the same street.

Recent work has considered alternative topologies that may better model urban areas. In [19], an approach to determine LOS and NLOS BSs by approximating a *LOS ball* was proposed. The model was shown to be able to better approximate the LOS area than [18]. In [20], three-dimensional Poisson buildings were modeled using Poisson processes to characterize the correlated shadowing effects in urban buildings. The idea was to add one more dimension to the Manhattan Poisson line processes (MPLP), by modeling the floor locations as Poisson process. This allowed an exact characterization of coverage of in-door urban cellular networks. In [14], a stochastic geometry model in a Manhattan type network was analyzed, since it is a tractable yet realistic model for Manhattan type urban streets. The urban streets were modeled as

one-dimensional MPLP and the coverage probability was derived considering the penetration effects of buildings. Unfortunately, the results in [14] used a pathloss model mainly considering the penetration effects of signals through urban buildings, with a fixed loss for each penetration. This is not applicable for mmWave systems where penetration loss is high. In this thesis, we also use the MPLP for modeling the urban street distribution, but combined with a mmWave-specific channel model.

Urban mmWave channel modeling There is a vast body of literature concerning mmWave channel modeling in urban areas, see, e.g., [21] and references therein. One of the key characteristics of urban environment is the high density of streets and high-rise buildings. Since mmWave signals are very sensitive to blockage, which induces significant signal attenuation, LOS and NLOS links can have sharply different pathloss exponents, as was also shown in numerous measurements [5][22][23], and is reflected in the standardized channel models [24]. Investigations in a variety of environments showed that in general, penetration loss increases with carrier frequency. For modern buildings with steel concrete and energy saving windows, in particular, penetration through just one wall can incur losses on the order of 30 dB; therefore propagation *through* buildings is not a relevant effect in mmWave urban environments [25].

In [26], a spatially consistent pathloss model was proposed for urban mmWavechannels in microcells. Based on ray tracing, it was shown that the pathloss exponents differ from street to street and should be modeled as a

function of both the street orientation and the absolute location of the BS and user equipment (UE)[2]. Hence, the signal is seen as propagating along different streets, with diffraction effects happening at the corner, instead of penetrating through the urban buildings. The pathloss is summed up by the individual pathloss on different segments of the propagation paths, incorporating an additional loss at each corner. This shows that the Euclidean distance might not be a good measure to characterize the pathloss effects in urban microcell networks at mmWave. In this thesis, we adopt a modified pathloss model similar to [26] based on the Manhattan distance, which enables tractable analysis while still retaining the key features of the channel. In this thesis, we develop a tractable framework to characterize the downlink coverage performance of urban mmWave vehicular networks. In specific, we consider snapshots of the urban microcellular networks, without modeling vehicle mobility. This reduces the network to an urban mmWave microcellular networks. We model the location of urban streets by a MPLP. The width of the street is neglected, and herein the blockage effects of vehicles are not considered in the analysis. We extend our previous paper [27] to account for large antenna arrays and directional beamforming at mmWave. We use a modification of the sectorized antenna model for tractable analysis [13, 28] and apply the new pathloss model from [26]. The pathloss model is characterized by the Manhattan distance of the propagation link, which, with MPLP street modeling, yields tractable results for coverage analysis.

[2]Henceforth we assume a downlink so that receiver and UE can be used exchangeably.

Based on our model, we analyze coverage of randomly located UEs on the roads formed by the lines, which is different from the conventional approach where coverage is analyzed conditioned on the links being outdoors [13]. We adopt a new procedure in the calculation of coverage probability, compared to the previous work [13]. We analyze the coverage probability by first computing the cumulative distribution function (CDF) of association link gain and then the coverage probability conditioned on the associated link gain. By averaging over the conditioned channel gain, we obtain simple but accurate expression of coverage probability. We also examine the probability that the link is LOS.

Compared to [27], this thesis also includes the following contributions. Based on the coverage probability, we obtain useful insights concerning the scaling laws of coverage probability with street and BS intensities, the sensitivity to propagation environment changes of LOS/NLOS paths and the effects of LOS/NLOS interference. Also, we derive closed-form expression of the LOS BS association probability. We then use the data of real streets in Chicago from *OpenStreetMap* [29–31] and extract it using Geographical Information System (GIS) application *QGIS* [32]. This is used to compare the ergodic rate of realistic streets, MPLP street model and fixed grid models, and MPLP-based analysis is validated for an outdoor microcell urban network at mmWave.

Chapter 2

System Model

In this section, we explain the key assumptions and models adopted in this thesis. First, we explain the street model in urban vehicular networks. Then, we introduce a modified mmWave sectorized antenna pattern used for the analysis. We present a tractable form of the pathloss model of mmWave microcells based on Manhattan distance from [26]. Lastly, we formulate the signal-to-interference-plus-noise ratio (SINR) of the receiver and demonstrate the strongest propagation path rule.

2.1 Network Model: MPLP model

We model the urban area as a stochastic Manhattan type network [14], [33], [34], and the location of the urban streets are modeled by Manhattan Poisson line process (MPLP). We show in Fig. 2.1 an illustration of the Manhattan network in Cartesian coordinate system, with origin denoted as O. Without loss of generality, a *typical* receiver is placed at O. Then, instead of modeling streets with fixed spacings in urban areas, we consider the location of both the cross and parallel streets to be stochastic. We generate two individual homogeneous Poisson point processes (PPP) as Ψ_x and Ψ_y, with

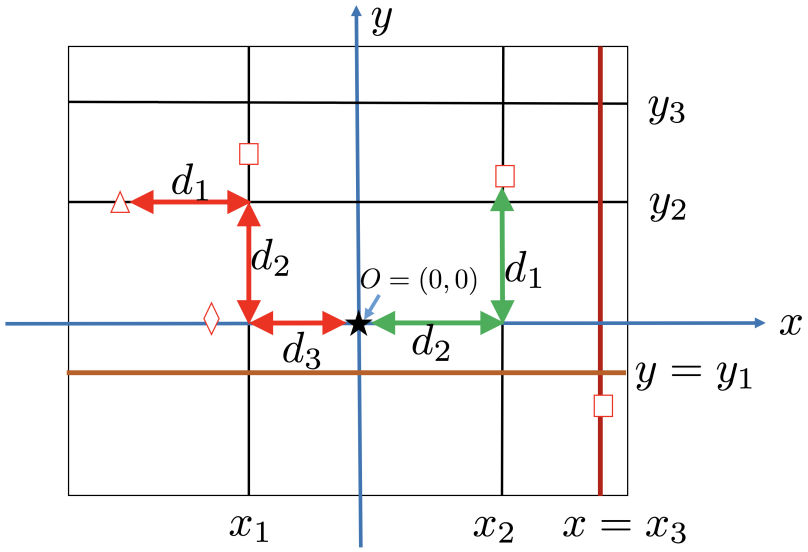

Figure 2.1: An illustration of our proposed pathloss model under the Cartesian coordinate system. Streets are represented by either $x = x_i$ (cross streets) or $y = y_i$ (parallel streets). The ★ is the typical receiver, the diamond ⋄ represents one typical BS, □ is a cross BS and △ is a parallel BS. The red line denotes the shortest propagation link of a parallel BS and the green line is the shortest propagation path of a cross BS. The pathloss in decibel scale is added up by the pathloss on each individual segments of the propagation path.

identical street intensity as λ_{S}. The streets are assumed to be either perfectly horizontal or vertical in the given coordinate system. Under the current coordinate system, we define the *parallel* streets as *parallel* to the x-axis, and $\bigcup_{y_i \in \Psi_y} y = y_i$, and *cross* streets as *perpendicular* to x-axis, and $\bigcup_{x_j \in \Psi_x} x = x_j$, where $\bigcup$ represents the union of sets. By Slivnyak's theorem [14], [33], the *typical* street $y = 0$ is added to the process. In particular, we neglect the street width in this thesis. BSs on the typical/cross and parallel streets are also modeled as independent one-dimensional homogeneous PPPs, where we assume that BS intensities on each street are identical, which is λ_{B}.

2.2 Sectorized antenna model

To leverage array gains, directional beamforming by multiple antennas are performed at mmWave BSs. For simplicity, we assume the receiver has an omni-directional antenna, and the BSs are equipped with N_{t} transmit antennas. Fig. 2.2 illustrates the sectorized antenna model adopted in this thesis [13], [28]. The beamwidth of the main lobe is θ and all the other directions outside the main lobe are assumed to be in the side lobe. In addition, we assume the antenna gains are identical G for all directions in the main lobe, and the same as g for all the side lobe directions.

We denote the pointing direction of the center of antenna main lobe as ϕ_1, and the direction to the receiver from the BS as ϕ_2. The receiver can either be aligned with the main lobe when ϕ_2 lies inside the main lobe, i.e., $|\phi_2-\phi_1| < \frac{\theta}{2}$, or aligned with the side lobe, when $|\phi_2-\phi_1| > \frac{\theta}{2}$. In the analysis of mmWave, uniformly beam angular distribution is widely accepted in pioneering work of mmWave cellular network analysis with stochastic geometry [13, 17, 35], which is also adopted in this thesis. Since the beamforming direction of the BS is assumed to be uniformly distributed in $\phi_1 \sim \text{uniform}(0, 2\pi)$, we have $\phi_2 - \phi_1 \sim \text{uniform}(0, 2\pi)$. Hence, the beamforming antenna gain $\mathcal{G}$ of one typical BS with LOS visibility to the typical receiver can be formulated by

$$\mathcal{G}(\phi_2 - \phi_1) = \mathbb{1}_{\phi_2-\phi_1\in(-\frac{\theta}{2},\frac{\theta}{2})}G + \left(1 - \mathbb{1}_{\phi_2-\phi_1\in(-\frac{\theta}{2},\frac{\theta}{2})}\right) g. \tag{2.1}$$

Since $\phi_2 - \phi_1 \sim \text{uniform}(0, 2\pi)$, the beamforming gain in (2.1) becomes

$$\mathcal{G} = \mathbb{I}(p)G + (1 - \mathbb{I}(p))g, \tag{2.2}$$

where $\mathbb{I}(p)$ is the Bernoulli random variable with parameter p, with

$$p = \frac{\theta}{2\pi}. \tag{2.3}$$

For a uniform planar array (UPA), the main lobe gain can be approximated by $G = N_{\mathrm{t}}$, which is the maximum power gain that can be supported with N_{t}-element antenna array. The side-lobe gain is approximated by $g = \frac{\sqrt{N_{\mathrm{t}}} - \frac{\sqrt{3}}{2\pi} N_{\mathrm{t}} \sin\left(\frac{\sqrt{3}}{2\sqrt{N_{\mathrm{t}}}}\right)}{\sqrt{N_{\mathrm{t}}} - \frac{\sqrt{3}}{2\pi} \sin\left(\frac{\sqrt{3}}{2\sqrt{N_{\mathrm{t}}}}\right)}$ [28].

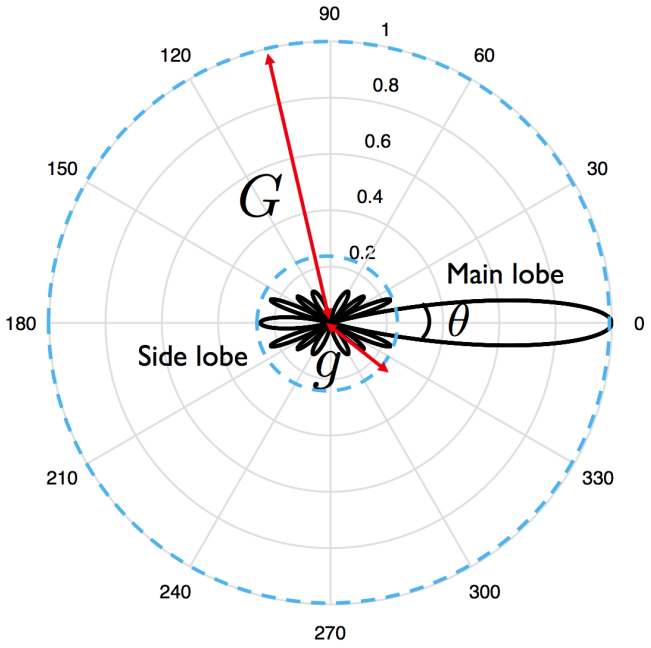

Figure 2.2: An illustration of the simplified sectorized antenna pattern. The example is drawn from a uniform linear array (ULA) with transmit antenna number $N_{\mathrm{t}} = 8$. We only consider the main lobes and the side lobes. Main lobes and side lobes are assumed to have identical gain on different directions, respectively denoted by G and g.

2.3 Pathloss model

We adopt a pathloss model that is based on the Manhattan distance instead of Euclidean distance. The model is similar to [26], but uses several modifications to provide tractability. Ray tracing shows that in an urban microcell, Euclidean distance might not be a dominant parameter in pathloss modeling. Instead, the street orientation relative to the BS location, and the absolute position of the BS and receiver are the key parameters to determine the pathloss.

It is shown by the ray tracing results that to calculate the pathloss of a propagation link in urban mmWave microcells, the pathloss on different segments of the propagation paths should be added up, with an additional loss when the waves couple into a new street canyon, in urban mmWave microcells. We assume that there are in total M segments of the propagation paths, i.e., $M-1$ corners along the propagation path where signal change directions. Note that the value of M depends on the actual position of the BS and the receiver. The individual length of the ith segment is denoted as d_i, the pathloss exponent on the ith segment is α_i, the corner loss at the corner of the ith the street segment and $i+1$th segment is Δ (in decibel scale), where we assume corner losses at different corners are identical.

We define the *LOS segment* as the first segment of the propagation path from the BS and *NLOS segment* as the remaining segments on the propagation path. We assume that LOS segments on different streets share the same pathloss exponent α_{L}, while the pathloss exponent for NLOS segments

is α_{N}.

Considering the sectorized antenna model at the BS, in this thesis, we redefine the pathloss as added by an extra beamforming gain besides the distance-based large scale fading, as

$$\mathrm{PL}_{\mathrm{dB}} = 10\left(\alpha_{\mathrm{L}} \log_{10} d_1 + \alpha_{\mathrm{N}} \sum_{i=2}^{M} \log_{10} d_i\right) + (M-1)\Delta - \mathcal{G}_{\mathrm{dB}}, \tag{2.4}$$

where the last term $\mathcal{G}_{\mathrm{dB}}$ is the random beamforming gain of the sectorized antenna model from (2.1) in decibel scale. With this Manhattan distance based pathloss model, we can classify the BSs into three categories, as illustrated in Fig. 2.1: i) BSs on the typical street (typical BSs) that have one direct propagation path to the typical receiver; ii) NLOS BSs on the cross streets (cross BSs) that have a propagation path consisting of a LOS segment (green path d_1) and NLOS segment (green path d_2) to the typical receiver, and iii) NLOS BSs on the parallel streets (parallel BSs) that have a propagation path consisting of a LOS segment (red path d_1) and two NLOS segments (red path d_2, d_3). This pathloss model also bears a strong relationship to [36], which considered the pathloss model in urban microcells where waves are coupled at the street corners with different angles.

2.4 Signal-to-interference-plus-noise ratio (SINR)

SINR coverage analysis is important to determine outage holes and ergodic throughput of the system. While these metrics in the context of mmWave-based vehicular networks depend on both mobility and the block-

age effects due to the vehicles, as mentioned before, in this thesis we simply consider snapshots of the urban microcelluar network and look at the distribution of the instantaneous SINR. This approach is taken primarily to confirm the analytic tractability of the pathloss model described in Section 2.3, which captures the blockage and shadowing effects due to buildings and accounts for the geometry of streets in an urban environment.

Based on the pathloss model in Section 2.3, there are three types of BSs to analyze: typical/cross/parallel BSs. To formulate the SINR, we first make the following assumption of the BS association rule.

Assumption 2.4.1. *The receiver is associated to the BS with the smallest pathloss, as defined in (2.4).*

We use Φ_{T} to denote the set of LOS link distances x_{T} from the typical BSs to the receiver. The set of lengths of the horizontal and vertical links, x_{C} (d_1 in green) and y_{C} (d_2 in green), constituting the propagation path from the cross BSs is denoted as Φ_{C}. Similarly, Φ_{P} is used to denote the set of distances $(x_{\mathrm{P}}, y_{\mathrm{P}}, z_{\mathrm{P}})$ (d_3, d_2, d_1 in red) corresponding to the propagation path from parallel BSs (see Fig. 2.1). To simplify demonstration, we define the path gain of the LOS and NLOS segment respectively as $\ell_{\mathrm{L}}(x)$ and $\ell_{\mathrm{N}}(x)$.

$$\ell_{\mathrm{L}}(x) = \mathcal{G} x^{-\alpha_{\mathrm{L}}}, \tag{2.5}$$

and

$$\ell_{\mathrm{N}}(x) = c x^{-\alpha_{\mathrm{N}}}, \tag{2.6}$$

where x is the length of the propagation segment, $\mathcal{G}$ is the random beamforming gain for each BS defined in (2.1). It should be noted that the beamforming gain is added only to the LOS segment pathloss. This is based on the definition that the LOS segment is the first path from the BS, hence with beamforming gain included; the corner loss term $c = 10^{-\Delta/10}$ in the total path gain expression is also captured along with the propagation loss in the NLOS segment in (2.6), with α_{N} denoting the NLOS pathloss exponent.

Conditioning on the associated link gain as u, the SINR can be formulated as follows, in terms of interference components, respectively from the typical BSs $I_{\phi_{\mathrm{T}}}$, cross BSs $I_{\phi_{\mathrm{C}}}$ and parallel BSs $I_{\phi_{\mathrm{P}}}$,

$$\mathrm{SINR} = \frac{h_o u}{N_0 + I_{\phi_{\mathrm{T}}}(o) + I_{\phi_{\mathrm{C}}}(o) + I_{\phi_{\mathrm{P}}}(o)}, \tag{2.7}$$

$$\text{with } I_{\phi_{\mathrm{T}}}(o) = \sum_{x_{\mathrm{T}}^i \in \Phi'_{\mathrm{T}}} h_i \ell_{\mathrm{L}}(x_{\mathrm{T}}^i), \tag{2.8}$$

$$I_{\phi_{\mathrm{C}}}(o) = \sum_{(x_{\mathrm{C}}^i, y_{\mathrm{C}}^i) \in \Phi'_{\mathrm{C}}} h_i \ell_{\mathrm{N}}(x_{\mathrm{C}}^i) \ell_{\mathrm{L}}(y_{\mathrm{C}}^i), \tag{2.9}$$

$$\text{and } I_{\phi_{\mathrm{P}}}(o) = \sum_{(x_{\mathrm{P}}^i, y_{\mathrm{P}}^i, z_{\mathrm{P}}^i) \in \Phi'_{\mathrm{P}}} h_i \ell_{\mathrm{N}}(x_{\mathrm{P}}^i) \ell_{\mathrm{N}}(y_{\mathrm{P}}^i) \ell_{\mathrm{L}}(z_{\mathrm{P}}^i), \tag{2.10}$$

where h_o is the small scale fading of the typical receiver from the associated BS and h_i is the small scale fading of the ith BS of the Poisson point processes.

Based on Assumption 2.4.1 and conditioning on the associated link gain as u, we have the following constraints for the set $\Phi'_{\mathrm{T}}, \Phi'_{\mathrm{C}}$ and Φ'_{P} in (2.8) – (2.10) as

$$\Phi'_{\mathrm{T}} = \{x_{\mathrm{T}} \in \Phi_{\mathrm{T}} \Big| \ell_{\mathrm{L}}(x_{\mathrm{T}}) < u\}, \tag{2.11}$$

$$\Phi'_{\mathrm{C}} = \{(x_{\mathrm{C}}, y_{\mathrm{C}}) \in \Phi_{\mathrm{C}} \Big| \ell_{\mathrm{N}}(x_{\mathrm{C}})\ell_{\mathrm{L}}(y_{\mathrm{C}}) < u\}, \tag{2.12}$$

$$\text{and } \Phi'_{\mathrm{P}} = \{(x_{\mathrm{P}}, y_{\mathrm{P}}, z_{\mathrm{P}}) \in \Phi_{\mathrm{P}} \Big| \ell_{\mathrm{N}}(x_{\mathrm{P}})\ell_{\mathrm{N}}(y_{\mathrm{P}})\ell_{\mathrm{L}}(z_{\mathrm{P}}) < u\}. \tag{2.13}$$

The above constraints are based on the strongest BS association rule in Assumption 2.4.1, all interfering BSs should have smaller path gain than u, which leads to (2.8) – (2.10).

2.4.1 Analysis of strongest path

Though there could be multiple propagation paths to the typical receiver and the actual received power is the sum of received signal power from different paths, to make the analysis tractable, we have the following assumption.

Assumption 2.4.2. *There is one unique path from any BS to the typical receiver (for analysis), which provides the smallest pathloss (with beamforming gain).*

To be the strongest path, the path should have i) shorter individual path segment lengths, ii) fewer individual segments, hence fewer corners and smaller corner loss (pathloss is calculated by multiplying individual segment pathloss and one extra multiplication might reduce the pathloss by orders of magnitude), iii) larger beamforming gain. The strongest path analysis is not straightforward when including the beamforming gain. For example, Fig. 2.3 and Fig. 2.4 demonstrate potential strongest paths of typical and cross BSs. In each of the cases, there is one *direct* path which has fewer corners and

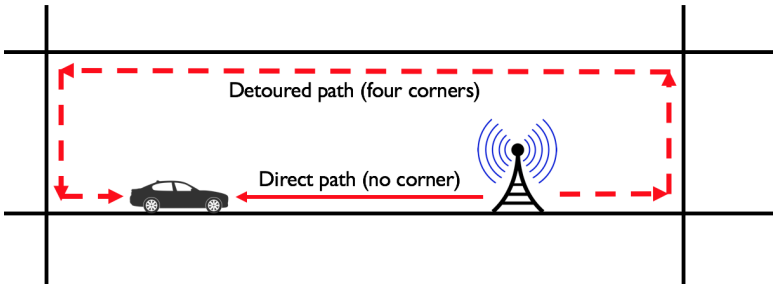

Figure 2.3: An illustration of the strongest path of typical BSs.

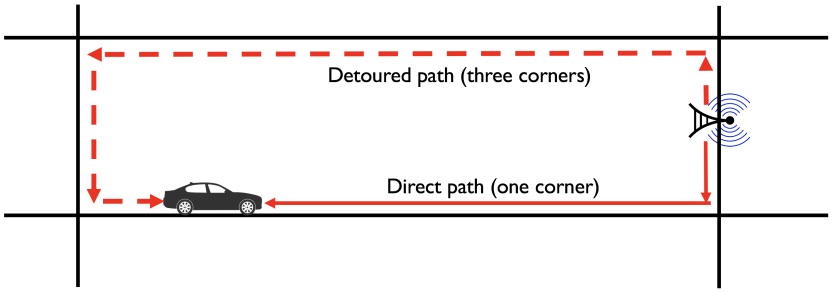

Figure 2.4: An illustration of the strongest path of cross BSs.

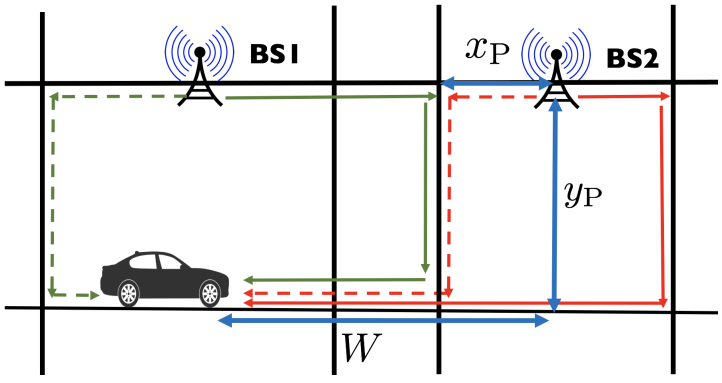

Figure 2.5: An illustration of the strongest path of parallel BSs.

one *detoured* path which detours its way before reaching the receiver. For typical BSs, the detoured path has *four* more corners than the direct path; while for the cross BSs, there are *two* more corners. Each corner introduces an approximately extra 20dB loss, while is much more significant than the effects compensated by the beamforming gain difference. Therefore, even if the main lobe beam is pointing in the detoured path direction, the strongest path should still be the direct path.

For the parallel BSs, one difference here is that both the detoured and direct paths have two corners, which makes it hard to select out the strongest path (see Fig. 2.5). In addition, the BS could either be in the *same block* as the receiver or *different block* as the receiver, as shown in Fig. 2.5. The two types of BSs show completely different selection rule of the strongest path. For the same block BS, it is clear that the strongest path could either be the green dashed line or the green solid line. For the different block BS, however, the strongest path could traverse any of the cross BSs and could point either left for right. To make the analysis tractable, we first make the following assumption.

Assumption 2.4.3. *For the strongest path of the parallel BSs, the signal travels along the LOS segment (first segment of the path) in the direction towards the receiver, rather than away from it.*

With this assumption, to find the strongest path for the parallel BS at different blocks as the receiver, we provide the following proposition.

Proposition 1. The strongest propagation path from a parallel BS is via either the cross street Θ_{R} closest to the receiver or Θ_{B} closest to the BS.

Proof. Conditioning on the location of the parallel BS, the segment y_{P} and the corner loss 2Δ of all propagation paths are the same, hence, the pathloss on the vertical link and the two corner losses can be taken out while formulating the following optimization problem.

Since $\mathcal{G}$ is a random variable taking values of G or g, as defined in (2.1), we have $\mathcal{G} \leq G$. Hence, the maximum path gain of the parallel BS G_{p} can be upper bounded by

$$\begin{aligned} G_{\mathrm{P}} &\leq G - 2\Delta - 10\alpha_{\mathrm{N}} \log_{10} y_{\mathrm{P}} + 10 G_{\mathrm{M}} \\ &\leq G - 2\Delta - 10\alpha_{\mathrm{N}} \log_{10} y_{\mathrm{P}} + 10 \max\left\{G_{\mathrm{M}}\right\}. \end{aligned} \tag{2.14}$$

where

$$G_{\mathrm{M}} = -\alpha_{\mathrm{N}} \log_{10} x_{\mathrm{P}} - \alpha_{\mathrm{L}} \log_{10} z_{\mathrm{P}}. \tag{2.15}$$

We then formulate the optimization problem of G_{M} as

$$\begin{aligned} \underset{x_{\mathrm{P}}, z_{\mathrm{P}} \in (0,W)}{\text{maximize}} \quad & -\alpha_{\mathrm{N}} \log_{10} x_{\mathrm{P}} - \alpha_{\mathrm{L}} \log_{10} z_{\mathrm{P}} \\ \text{subject to} \quad & x_{\mathrm{P}} + z_{\mathrm{P}} = W \end{aligned} \tag{2.16}$$

The objective function can be expressed as $P(x) = -\alpha_{\mathrm{N}} \log x - \alpha_{\mathrm{L}} \log(W - x)$, $x \in (0, W)$, whose second order derivative is

$$P''(x) = \frac{\alpha_{\mathrm{N}}}{x^2} + \frac{\alpha_{\mathrm{L}}}{(W-x)^2}, \tag{2.17}$$

The second order derivative of $P(x)$ is positive for all α_{L}, α_{N}, and W, which means $P(x)$ is convex. Denoting the distance from Θ_{R} to the receiver as x_1 and the distance from Θ_{B} to the BS as x_2, and using the convexity of $P(x)$, we have

$$\begin{aligned} &P(\lambda x_1 + (1-\lambda)x_2) < \lambda P(x_1) + (1-\lambda)P(x_2) \\ &< \max\{P(x_1), P(x_2)\} \ \ \forall \lambda \in (0,1) \text{ and } x_1, x_2 \in (0, W). \end{aligned} \tag{2.18}$$

In (2.18), $P(\lambda x_1 + (1-\lambda)x_2)$ parameterizes all path gains of the propagation paths via any cross street lying between Θ_{R} and Θ_{B}. From the second inequality in (2.18), all these propagation paths have smaller path gain than that going through the streets specified in this proposition, which concludes the proof. □

Since the pathloss exponent of the segment z_{P} is α_{L} and that of the segment x_{P} is α_{N}, with $\alpha_{\mathrm{L}} < \alpha_{\mathrm{N}}$, it is intuitive that the strongest path is more likely to be via the street *closest to the receiver*, i.e., Θ_{R}.

To conclude the discussion on the uniqueness of the propagation path in the system model considered in this thesis, we demonstrated that for both the typical and cross BSs, the propagation path is unique and also easy to identify based on the strongest path gain association criterion. For the parallel BS, irrespective of whether the BS is located in the same block as the receiver, there are only two potential paths to be the strongest, and for analysis, we choose the path which traverses the cross street that is closest to the receiver.

Chapter 3

Coverage Analysis

In this section, we compute the coverage probability of a typical receiver in the MPLP microcellular network. First, we explain the independent thinning of the BSs considering the sectorized beam pattern of the mmWave BSs. Then, we analyze the CDF of the associated link path gain based on strongest BS association rule in Assumption 2.4.1. In addition, we derive an accurate and concise expression of the coverage probability. Finally, we examine the effects of LOS and NLOS interference in MPLP network.

3.1 Independent thinning of BSs

Based on the sectorized antenna model in Section 2.2, the BSs are thinned with probability p_{T} and $1-p_{\mathrm{T}}$, respectively, which then generate two independent Poisson point processes of BSs with antenna gain of G and g respectively. After the independent thinning, the densities of the independent thinning of BSs with antenna gain of G and g are respectively

$$\lambda_{\mathrm{b}} = p_{\mathrm{T}}\lambda_{\mathrm{B}} \quad \text{and} \quad \bar{\lambda}_{\mathrm{b}} = (1-p_{\mathrm{T}})\lambda_{\mathrm{B}}. \tag{3.1}$$

For typical and cross BSs, the thinning probability is $p_{\mathrm{T}} = p$, which is the probability that the receiver lies inside the main lobe, as defined in (2.3). This

is based on the analysis of the strongest path in Section 2.4.1. For the typical BSs, the thinning probability is obvious; for the cross BSs, we assume only the BSs that are pointing towards the corner aligned with the typical street have beamforming gain as G. Hence, typical and cross BSs have identical thinning probability.

For the parallel BSs, as is shown in Section 2.4.1, we provide an approximation by bounding the path gain of the parallel BS G_{P} by assuming all of the parallel BSs' main lobe beams are pointing towards receiver, i.e., we assume all of the parallel BSs have beamforming gain as G. Hence, the result of the thinning probability simply reduces to $p_{\mathrm{T}} = 1$.

3.2 Distribution of associated link gain

To simplify SINR coverage analysis, we assume all links experience independent and identically distributed (I.I.D.) Rayleigh fading with mean 1, $h \sim \exp(1)$. We denote the normalized transmit power $P_{\mathrm{B}} = 1$ and represent the noise by N_0. Since the SINR expression in (2.7) is conditioned on the associated link gain u, we first analyze the distribution of u. Based on the BS association law in Assumption 2.4.1, the receiver can be associated to either a typical/cross or parallel BS. The following lemma provides the cumulative density function (CDF) of the largest gain from the typical/cross/parallel BS respectively.

Lemma 3.2.1. *The CDFs of the largest gain of the typical BSs* $u_1 = \max_{(x_{\mathrm{T}} \in \Phi_{\mathrm{T}})} \{\ell_{\mathrm{L}}(x_{\mathrm{T}})\}$*, cross BSs* $u_2 = \max_{(x_{\mathrm{C}}, y_{\mathrm{C}}) \in \Phi_{\mathrm{C}}} \{\ell_{\mathrm{N}}(x_{\mathrm{C}})\ell_{\mathrm{L}}(y_{\mathrm{C}})\}$ *and*

parallel BSs $u_3 = \max_{(x_\mathrm{P},y_\mathrm{P},z_\mathrm{P})\in\Phi_\mathrm{P}}\{\ell_\mathrm{N}(x_\mathrm{P})\ell_\mathrm{N}(y_\mathrm{P})\ell_\mathrm{L}(x_\mathrm{P})\}$ *are given or bounded by*

$$F_{u_\mathrm{T}}(u) = \exp\left(-\gamma_\mathrm{T}\lambda_\mathrm{B}u^{-\frac{1}{\alpha_\mathrm{L}}}\right), \tag{3.2}$$

$$F_{u_\mathrm{C}}(u) = \exp\left(-\gamma_\mathrm{C}\lambda_\mathrm{B}^{\frac{\alpha_\mathrm{L}}{\alpha_\mathrm{T}}}u^{-\frac{1}{\alpha_\mathrm{N}}}\right), \tag{3.3}$$

$$F_{u_\mathrm{P}}(u) \gtrsim 2\lambda_\mathrm{S}\sqrt{\frac{2\gamma_\mathrm{P}\lambda_\mathrm{B}^{\frac{\alpha_\mathrm{L}}{\alpha_\mathrm{N}}}u^{-\frac{1}{\alpha_\mathrm{N}}}}{\lambda_\mathrm{S}}}K_1\left(2\sqrt{2\gamma_\mathrm{P}\lambda_\mathrm{S}\lambda_\mathrm{B}^{\frac{\alpha_\mathrm{L}}{\alpha_\mathrm{N}}}u^{-\frac{1}{\alpha_\mathrm{N}}}}\right), \tag{3.4}$$

where

$$\gamma_\mathrm{T} = 2p_\mathrm{T}G^{\frac{1}{\alpha_\mathrm{L}}} + 2(1-p_\mathrm{T})g^{\frac{1}{\alpha_\mathrm{L}}}, \tag{3.5}$$

$$\gamma_\mathrm{C} = 2\lambda_\mathrm{S}\gamma_\mathrm{T}^{\frac{\alpha_\mathrm{L}}{\alpha_\mathrm{N}}}c^{\frac{1}{\alpha_\mathrm{N}}}\Gamma\left(1-\frac{\alpha_\mathrm{L}}{\alpha_\mathrm{N}}\right), \tag{3.6}$$

$$\gamma_\mathrm{P} = \frac{\gamma_\mathrm{C}2^{\frac{\alpha_\mathrm{L}}{\alpha_\mathrm{N}}}G^{\frac{1}{\alpha_\mathrm{N}}}c^{\frac{1}{\alpha_\mathrm{N}}}}{\gamma_\mathrm{T}^{\frac{\alpha_\mathrm{L}}{\alpha_\mathrm{N}}}}, \tag{3.7}$$

and $K_1(\cdot)$ *is the* 1*-st order modified Bessel's function of the second kind [37].*

Proof. Denote the PPP of the BSs on typical street with gain G as Ψ_T and with gain g as $\bar{\Psi}_\mathrm{T}$, then the CDF of the largest channel gain from BSs on the typical street is

$$\begin{aligned}
F_{u_\mathrm{T}}(u) &= \mathbb{P}\left(\max\left\{\max_{x\in\Psi_\mathrm{T}}Gx^{-\alpha_\mathrm{L}}, \max_{x\in\bar{\Psi}_\mathrm{T}}gx^{-\alpha_\mathrm{L}}\right\} < u\right) \\
&\overset{(a)}{=} \mathbb{P}\left(\max_{x\in\Psi_\mathrm{T}}Gx^{-\alpha_\mathrm{L}} < u\right)\mathbb{P}\left(\max_{x\in\bar{\Psi}_\mathrm{T}}gx^{-\alpha_\mathrm{L}} < u\right) \\
&= \mathbb{P}\left(\min_{x\in\Psi_\mathrm{T}}x > G^{\frac{1}{\alpha_\mathrm{L}}}u^{-\frac{1}{\alpha_\mathrm{L}}}\right)\mathbb{P}\left(\min_{x\in\bar{\Psi}_\mathrm{T}}x > g^{\frac{1}{\alpha_\mathrm{L}}}u^{-\frac{1}{\alpha_\mathrm{L}}}\right)
\end{aligned}$$

$$\overset{(b)}{=} \exp\left(-2\left(\lambda_{\mathrm{b}} G^{\frac{1}{\alpha_{\mathrm{L}}}} + \bar{\lambda}_{\mathrm{b}} g^{\frac{1}{\alpha_{\mathrm{L}}}}\right) u^{-\frac{1}{\alpha_{\mathrm{L}}}}\right)$$
$$\overset{(c)}{=} \exp\left(-2\lambda_{\mathrm{B}}\left(p_{\mathrm{T}} G^{\frac{1}{\alpha_{\mathrm{L}}}} + (1-p_{\mathrm{T}}) g^{\frac{1}{\alpha_{\mathrm{L}}}}\right) u^{-\frac{1}{\alpha_{\mathrm{L}}}}\right), \tag{3.8}$$

where (a) and (c) follows from the independent thinning of BSs on the typical street of BSs with different antenna gains, (b) is based on the distribution of closest distance to one fixed point of one-dimensional PPP with intensity λ, and $\min\{x\}$ follows an exponential distribution, with parameter, $\min\{x\} \sim \exp(2\lambda)$.

Similarly, for the CDF of the largest channel gain from the BSs on the cross streets, we consider the BSs with antenna gain as G first as

$$F_{u_{\mathrm{C}}^{\mathrm{G}}}(u) = \mathbb{E}_{\Phi_{\mathrm{C}}}\left[\prod^{(x_{\mathrm{C}},y_{\mathrm{C}}\in\Phi_{\mathrm{C}})} \mathbb{P}\left(x_{\mathrm{C}}^{-\alpha_{\mathrm{N}}} y_{\mathrm{C}}^{-\alpha_{\mathrm{L}}} c\mathcal{G} < u\right)\right]$$
$$= \mathbb{E}_{\Phi_{\mathrm{C}}}\left[\prod^{(x_{\mathrm{C}},y_{\mathrm{C}})\in\Phi_{\mathrm{C}}} \mathbb{P}\left(x_{\mathrm{C}}^{-\alpha_{\mathrm{N}}} \min(y_{\mathrm{C}})^{-\alpha_{\mathrm{L}}} c\mathcal{G} < u\right)\right]$$
$$\overset{(a)}{=} \mathbb{E}_{\Phi_{\mathrm{C}}}\left[\prod^{x_{\mathrm{C}}} \exp\left(-\lambda_{\mathrm{B}}\gamma_{\mathrm{T}} x_{\mathrm{C}}^{-\frac{\alpha_{\mathrm{N}}}{\alpha_{\mathrm{L}}}} c^{\frac{1}{\alpha_{\mathrm{L}}}} u^{-\frac{1}{\alpha_{\mathrm{L}}}}\right)\right]$$
$$\overset{(b)}{=} \exp\left(-2\lambda_{\mathrm{S}}\int_0^{\infty} 1 - \exp\left(-\lambda_{\mathrm{B}}\gamma_{\mathrm{T}} x^{-\frac{\alpha_{\mathrm{N}}}{\alpha_{\mathrm{L}}}} c^{\frac{1}{\alpha_{\mathrm{L}}}} u^{-\frac{1}{\alpha_{\mathrm{L}}}}\right) dx\right)$$
$$= \exp\left(-\gamma_{\mathrm{C}}\lambda_{\mathrm{B}}^{\frac{\alpha_{\mathrm{L}}}{\alpha_{\mathrm{N}}}} u^{-\frac{1}{\alpha_{\mathrm{N}}}}\right), \tag{3.9}$$

where (a) follows the void probability of the PPP and (b) is based on the probability generating functional (PGFL). Hence, by the independent thinning, the proof is concluded.

Here, we provide a lower bound of the CDF of the associated link path gain, where the lower bound is achieved when we assume the strongest path

has beamforming gain G. Also, from the demonstration in Section 2.4.1, the strongest path is always via the cross street closest to the receiver. Based on this assumption, the lower bound of the CDF can be derived as

$$\begin{aligned}
F_{u_{\mathrm{P}}}(u) &\gtrsim \mathbb{P}\left(\bigcap^{(x_{\mathrm{P}},y_{\mathrm{P}},z_{\mathrm{P}})\in\Phi_{\mathrm{P}}} x_{\mathrm{P}}^{-\alpha_{\mathrm{N}}} y_{\mathrm{P}}^{-\alpha_{\mathrm{N}}} z_{\mathrm{P}}^{-\alpha_{\mathrm{L}}} c^2 G < u\right) \\
&= \mathbb{E}_{x_{\mathrm{P}}}\left\{\prod^{y_{\mathrm{P}}} \exp\left(-2\lambda_{\mathrm{B}} G^{\frac{1}{\alpha_{\mathrm{L}}}} u^{-\frac{1}{\alpha_{\mathrm{L}}}} c^{\frac{2}{\alpha_{\mathrm{L}}}} x_{\mathrm{P}}^{-\frac{\alpha_{\mathrm{N}}}{\alpha_{\mathrm{L}}}} y_{\mathrm{P}}^{-\frac{\alpha_{\mathrm{N}}}{\alpha_{\mathrm{L}}}}\right)\right\} \\
&= \mathbb{E}_{x_{\mathrm{P}}}\left\{\exp\left(-\gamma_{\mathrm{P}} \lambda_{\mathrm{B}}^{\frac{\alpha_{\mathrm{L}}}{\alpha_{\mathrm{N}}}} x_{\mathrm{P}}^{-1}\right)\right\} \\
&= \int_0^\infty 2\lambda_{\mathrm{S}} \exp\left(-\gamma_{\mathrm{P}} \lambda_{\mathrm{B}}^{\frac{\alpha_{\mathrm{L}}}{\alpha_{\mathrm{N}}}} x^{-1} - 2\lambda_{\mathrm{S}} x\right) dx \\
&= 2\lambda_{\mathrm{S}} \sqrt{\frac{2\gamma_{\mathrm{P}} \lambda_{\mathrm{B}}^{\frac{\alpha_{\mathrm{L}}}{\alpha_{\mathrm{N}}}} u^{-\frac{1}{\alpha_{\mathrm{N}}}}}{\lambda_{\mathrm{S}}}} K_1\left(2\sqrt{2\gamma_{\mathrm{P}}\lambda_{\mathrm{S}}\lambda_{\mathrm{B}}^{\frac{\alpha_{\mathrm{L}}}{\alpha_{\mathrm{N}}}} u^{-\frac{1}{\alpha_{\mathrm{N}}}}}\right),
\end{aligned} \tag{3.10}$$

where $\bigcap$ denotes the intersection of all of the events defined in the set $(x_{\mathrm{P}}, y_{\mathrm{P}}, z_{\mathrm{P}}) \in \Phi_{\mathrm{P}}$, and the last equation follows from the equation [37].

$$\int_0^\infty \exp\left(\frac{\beta}{4x} - \gamma x\right) dx = \sqrt{\frac{\beta}{\gamma}} K_1\left(\sqrt{\beta\gamma}\right) \tag{3.11}$$

by simple calculate, we can conclude the proof. □

Based on properties of the modified Bessel function, when the argument μ of $K_1(\mu)$ becomes small, we can approximate it as [38]

$$K_1(\mu) \sim \mu^{-1}. \tag{3.12}$$

Since γ_{P} scales with $\lambda_{\mathrm{S}}\lambda_{\mathrm{B}}^{\frac{\alpha_{\mathrm{L}}}{\alpha_{\mathrm{N}}}}$, which is generally very small, we have $\gamma_{\mathrm{P}} \ll 1$. Hence, the argument $\gamma_{\mathrm{P}}\lambda_{\mathrm{B}}^{\frac{\alpha_{\mathrm{L}}}{\alpha_{\mathrm{N}}}}$ inside the modified Bessel function in (3.4) is also

negligible. The corner loss term $c^{\frac{1}{\alpha_N}}$ further reduces the value to a large extent, so that (3.12) applies. Consequently, we can approximate (3.4) as

$$F_{u_P}(u) \approx 2\lambda_S \sqrt{\frac{2\gamma_P \lambda_B^{\frac{\alpha_L}{\alpha_N}} u^{-\frac{1}{\alpha_N}}}{\lambda_S}} \left(2\sqrt{2\gamma_P \lambda_S \lambda_B^{\frac{\alpha_L}{\alpha_N}} u^{-\frac{1}{\alpha_N}}} \right)^{-1} = 1, \tag{3.13}$$

which implies that generally the largest gain from a parallel BS is very small, that is, the probability of associating with a parallel BS is negligible.

Using Lemma 3.2.1, the distribution of the associated link path gain $\mathrm{U} = \max\{u_T, u_C, u_P\}$ can be evaluated as

$$\begin{aligned} F_U(u) &= \mathbb{P}\left(\max\{u_T, u_C, u_P\} < u\right) \\ &\overset{(a)}{=} \mathbb{P}\left(\max\{u_T\} < u\right) \mathbb{P}\left(\max\{u_C\} < u\right) \mathbb{P}\left(\max\{u_P\} < u\right) \\ &\overset{(b)}{\approx} \exp\left(-\gamma_T \lambda_B u^{-\frac{1}{\alpha_L}}\right) \exp\left(-\gamma_C \lambda_B^{\frac{\alpha_L}{\alpha_N}} u^{-\frac{1}{\alpha_N}}\right), \end{aligned} \tag{3.14}$$

where (a) is based on the fact that the locations of the typical/cross/parallel BSs are mutually independent, (b) follows the results of Lemma 3.2.1 that the association with parallel BSs is negligible.

We then give the parameters used in this thesis in Table 3.1. The simulation parameters are applicable to all of the following simulation results, unless stated otherwise.

Fig. 3.1 compares the numerically evaluated CDF of the associated link gain of association only with typical BSs, with typical/cross BSs and considering all association cases, against the theoretical result given in (3.14). It is seen that the analytic result matches well with the numerical result. It

Table 3.1: Simulation Parameters

PARAMETERS	VALUES
UPA Antenna Number N_{t}	8×8
LOS Pathloss Exponent α_{L}	2.5
NLOS Pathloss Exponent α_{N}	7
Corner Loss Δ	20dB
Intensity of Street λ_{S}	0.01
Intensity of BS λ_{B},	0.01

can also be seen that the empirical CDF curves obtained with and without the association with the parallel BSs coincide. This verifies the analysis in Lemma 3.2.1 and the subsequent approximation for largest gain seen by parallel BSs. Also, the curve shows that the cross BSs association is very small compared to the typical BSs association.

3.3 Coverage probability

In this section, we derive a closed-form expression for the coverage probability $p_{\mathrm{c}}(u, T)$ conditioned on the associated link gain as u. The coverage probability conditioned on u is defined as

$$p_{\mathrm{c}}(u, T) = \mathbb{P}\left(\mathrm{SINR} > T | u\right). \tag{3.15}$$

Using (2.7) – (2.10), (3.15) can be expanded in terms of the Laplace transforms of interference and noise as follows.

$$\begin{aligned} p_{\mathrm{c}}(u, T) &= \mathbb{P}\left(h > T u^{-1}(N_0 + I_{\phi_{\mathrm{T}}}(o) + I_{\phi_{\mathrm{V}}}(o) + I_{\phi_{\mathrm{H}}}(o))\right) \\ &\overset{(a)}{=} \exp(-T u^{-1} N_0) \mathcal{L}_{I_{\phi_{\mathrm{T}}}}(T u^{-1}) \mathcal{L}_{I_{\phi_{\mathrm{C}}} + I_{\phi_{\mathrm{P}}}}(T u^{-1}), \end{aligned} \tag{3.16}$$

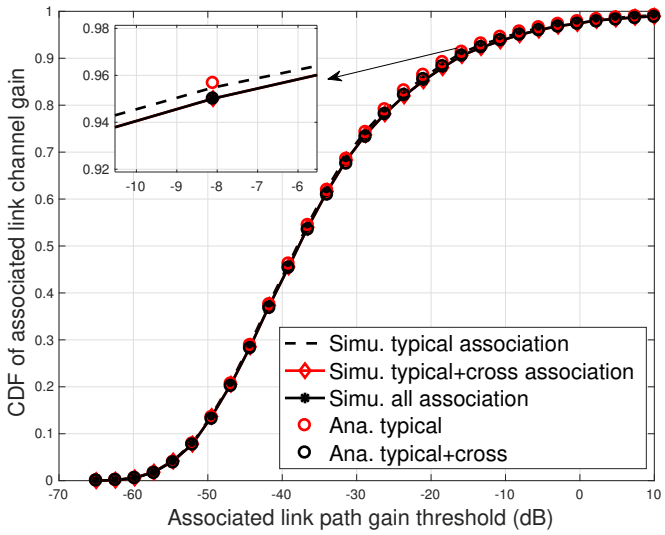

Figure 3.1: Comparison of analytic and numerical associated link gain distribution. The black dashed line represents the association with only the typical BSs, the red solid line is the CDF considering association with both typical and cross BSs, and the black solid line is the result of considering all association cases. The red circle and black circle respectively denote the analytic result of CDF of associated gain with only typical BS association and typical/cross BS association.

where (a) is based on the assumption of i.i.d. Rayleigh fading channels, and $\mathcal{L}_{(\cdot)}$ is the Laplace transform (LT) of random variable $(\cdot)$. Note that we cannot completely decouple the interference terms since the propagation links from the cross and parallel BSs share the same path segments thus making their individual interference not independent. To analyze the problem, we start with examining the parallel BS interference.

Proposition 2. A lower bound of LT of the interference from the parallel BSs

$I_{\phi_{\rm P}}$ is

$$\mathcal{L}_{I_{\phi_{\rm P}}}(T,u) \gtrsim 2\lambda_{\rm S}\sqrt{\frac{2\gamma_{\rm P}\left(\lambda_{\rm B}\varrho(T)\right)^{\frac{\alpha_{\rm L}}{\alpha_{\rm N}}}u^{-\frac{1}{\alpha_{\rm N}}}}{\lambda_{\rm S}}} \times K_1\left(2\sqrt{2\gamma_{\rm P}\lambda_{\rm S}\left(\lambda_{\rm B}\varrho(T)\right)^{\frac{\alpha_{\rm L}}{\alpha_{\rm N}}}u^{-\frac{1}{\alpha_{\rm N}}}}\right) \approx 1, \tag{3.17}$$

where $\gamma_{\rm P}$ is defined in (3.5), and

$$\varrho(T) = \int_1^\infty \frac{1}{1+T^{-1}\mu^{\alpha_{\rm L}}}d\mu. \tag{3.18}$$

Proof. The LT of the parallel BS is similar, and is given as follows.

$$\begin{aligned}
&\mathcal{L}_{I_{\phi_{\rm P}}}(Tu^{-1}) \\
&= \mathbb{E}_{\phi_{\rm P}}\left[\exp\left(-\sum_{(x_{\rm P},y_{\rm P},z_{\rm P})\in\Phi_{\rm P}} Tu^{-1}hx_{\rm P}^{-\alpha_{\rm N}}y_{\rm P}^{-\alpha_{\rm N}}z_{\rm P}^{-\alpha_{\rm L}}c^2G\right)\right] \\
&\overset{(a)}{=} \mathbb{E}_{x_{\rm P}}\left\{\prod^{y_{\rm P}}\exp\left(-2\lambda_{\rm B}G^{\frac{1}{\alpha_{\rm L}}}\varrho(T)u^{-\frac{1}{\alpha_{\rm L}}}c^{\frac{2}{\alpha_{\rm L}}}(xy)^{-\frac{\alpha_{\rm N}}{\alpha_{\rm L}}}\right)\right\} \\
&\overset{(b)}{=} \mathbb{E}_{x_{\rm P}}\left\{\exp\left(-\gamma_{\rm P}\varrho(T)^{\frac{\alpha_{\rm L}}{\alpha_{\rm N}}}\lambda_{\rm B}^{\frac{\alpha_{\rm L}}{\alpha_{\rm N}}}x_{\rm P}^{-1}\right)\right\} \\
&= \int_0^\infty 2\lambda_{\rm S}\exp\left(-\gamma_{\rm P}\varrho(T)^{\frac{\alpha_{\rm L}}{\alpha_{\rm N}}}\lambda_{\rm B}^{\frac{\alpha_{\rm L}}{\alpha_{\rm N}}}x^{-1}-2\lambda_{\rm S}x\right)dx \\
&= 2\lambda_{\rm S}\sqrt{\frac{2\gamma_{\rm P}\varrho(T)^{\frac{\alpha_{\rm L}}{\alpha_{\rm N}}}\lambda_{\rm B}^{\frac{\alpha_{\rm L}}{\alpha_{\rm N}}}}{\lambda_{\rm S}}}K_1\left(2\sqrt{2\gamma_{\rm P}\varrho(T)^{\frac{\alpha_{\rm L}}{\alpha_{\rm N}}}\lambda_{\rm B}^{\frac{\alpha_{\rm L}}{\alpha_{\rm N}}}}\right),
\end{aligned} \tag{3.19}$$

where (a) and (b) follow the traditional procedures in analysis of stochastic geometry and are similar to the proof of Laplace transform of $I_{\phi_{\rm T}}$ and $I_{\phi_{\rm C}}$ above.

□

Since the LT of the parallel interference evaluates to 1 approximately, which indicates that the interference from parallel BSs is small enough to be neglected, i.e., $I_{\phi_{\mathrm{P}}} \approx 0$. Hence, the coverage probability in (3.20) can be reformulated as

$$p_{\mathrm{c}}(u,T) = \exp(-Tu^{-1}N_0)\mathcal{L}_{I_{\phi_{\mathrm{T}}}}(Tu^{-1})\mathcal{L}_{I_{\phi_{\mathrm{C}}}}(Tu^{-1}), \tag{3.20}$$

which is derived in the following Theorem.

Theorem 3.3.1. *The coverage probability conditioned on the channel gain u of the associated link is*

$$p_{\mathrm{c}}(u,T) = \exp(-\beta_1 u^{-1})\exp(-\beta_2\lambda_{\mathrm{B}}u^{-\frac{1}{\alpha_{\mathrm{L}}}})\exp\left(-\beta_3\lambda_{\mathrm{B}}^{\frac{\alpha_{\mathrm{L}}}{\alpha_{\mathrm{N}}}}u^{-\frac{1}{\alpha_{\mathrm{N}}}}\right), \tag{3.21}$$

where

$$\beta_1 = TN_0, \quad \beta_2 = \gamma_{\mathrm{T}}\varrho(T), \quad \beta_3 = \gamma_{\mathrm{C}}\varrho(T)^{\frac{\alpha_{\mathrm{L}}}{\alpha_{\mathrm{N}}}}, \tag{3.22}$$

and $\varrho(T)$ is defined in (3.18).

Proof. We respectively give the LT of the typical and cross interference $I_{\phi_{\mathrm{T}}}$, $I_{\phi_{\mathrm{C}}}$. The LT of the typical BS interference $\mathcal{L}_{I_{\phi_{\mathrm{T}}}}(s)$ with beamforming gain as G can be given by

$$\begin{aligned}
\mathcal{L}_{I_{\phi_{\mathrm{T}}}}(s) &= \mathbb{E}\left[\exp\left(-s\sum_{x_{\mathrm{T}}\in\Phi_{\mathrm{T}}} hx_{\mathrm{T}}^{-\alpha_{\mathrm{L}}}\right)\right] \\
&= \exp\left(-2\lambda_{\mathrm{b}}\int_{\left(\frac{u}{G}\right)^{-\frac{1}{\alpha_{\mathrm{L}}}}}^{\infty}\mathbb{E}\left(1-\exp\left(-sGhx_{\mathrm{T}}^{-\alpha_{\mathrm{L}}}\right)\right)\right) \\
&= \exp\left(-2\lambda_{\mathrm{b}}\int_{\left(\frac{u}{G}\right)^{-\frac{1}{\alpha_{\mathrm{L}}}}}^{\infty}\frac{1}{1+s^{-1}G^{-1}x_{\mathrm{T}}^{\alpha_{\mathrm{L}}}}dx_{\mathrm{T}}\right).
\end{aligned} \tag{3.23}$$

Then plugging in $s = Tv^{-1}$ and by change of variables $\mu = x\left(\frac{u}{G}\right)^{\frac{1}{\alpha_{\mathrm{L}}}}$ the result can be simplifed by

$$\mathcal{L}_{I_{\phi_{\mathrm{T}}}}(s) = \exp\left(-\gamma_{\mathrm{T}}\lambda_{\mathrm{B}}u^{-\frac{1}{\alpha_{\mathrm{L}}}}\int_1^{\infty}\frac{1}{1+T^{-1}\mu^{\alpha_{\mathrm{L}}}}d\mu\right). \tag{3.24}$$

The LT of the NLOS interferers on cross streets with beamforming gain G follows the similar proof above and proof of $I_{\phi_{\mathrm{T}}}$, which is

$$\begin{aligned}
\mathcal{L}_{I_{\phi_{\mathrm{C}}}}(s) &= \mathbb{E}\left[\exp\left(-\sum_{(x_{\mathrm{C}},y_{\mathrm{C}})\in\Phi_{\mathrm{C}}} shx_{\mathrm{C}}^{-\alpha_{\mathrm{N}}}y_{\mathrm{C}}^{-\alpha_{\mathrm{L}}}cG\right)\right] \\
&= \mathbb{E}\left[\prod_{x_{\mathrm{C}}}\exp\left(-\gamma_{\mathrm{T}}\lambda_{\mathrm{B}}x_{\mathrm{C}}^{-\frac{\alpha_{\mathrm{N}}}{\alpha_{\mathrm{L}}}}u^{-\frac{1}{\alpha_{\mathrm{L}}}}c^{\frac{1}{\alpha_{\mathrm{L}}}}\varrho(T)\right)\right] \\
&= \exp\left(-2\lambda_{\mathrm{S}}\left(\gamma_{\mathrm{T}}\lambda_{\mathrm{B}}c^{\frac{1}{\alpha_{\mathrm{L}}}}\varrho(T)\right)^{\frac{\alpha_{\mathrm{L}}}{\alpha_{\mathrm{N}}}}\Gamma\left(1-\frac{\alpha_{\mathrm{L}}}{\alpha_{\mathrm{N}}}\right)u^{-\frac{1}{\alpha_{\mathrm{N}}}}\right).
\end{aligned} \tag{3.25}$$

□

Using Theorem 3.3.1 and the distribution of the associated link path gain in (3.14), the SINR coverage probability can be evaluated as

$$P_{\mathrm{c}}(T) = \int_0^{\infty} p_{\mathrm{c}}(u,T)f_{\mathrm{U}}(u)du, \tag{3.26}$$

where $p_{\mathrm{c}}(u,T)$ is provided in (3.21), and the probability density function (PDF) $f_{\mathrm{U}}(u)$ can be obtained from the CDF derived in (3.14).

3.3.1 The effect of LOS and NLOS interferers

In Proposition 2, we showed that the parallel BSs interference can be neglected in the analysis. In this section, we further compare the effects of

typical interference $I_{\phi_{\mathrm{T}}}$ and cross interference $I_{\phi_{\mathrm{C}}}$. For tractable analysis, we assume the receiver is associated to the typical BS, so that we can have simpler associated link gain distribution. The analysis is based on the application of Jensen's inequality to the individual LT of $I_{\phi_{\mathrm{T}}}$ and $I_{\phi_{\mathrm{C}}}$.

From Theorem 1, the LT of the interference of BSs on the typical street is $\mathcal{L}_{I_{\phi_{\mathrm{T}}}}(T,u) = \mathbb{E}_u\left[\exp\left(-\beta_2\lambda_{\mathrm{B}}u^{-\frac{1}{\alpha_{\mathrm{L}}}}\right)\right]$ and the LT of the interference due to the NLOS BSs on the cross streets is $\mathcal{L}_{I_{\phi_{\mathrm{C}}}}(T,u) = \mathbb{E}_u\left[\exp\left(-\beta_3\left(\lambda_{\mathrm{B}}u^{-\frac{1}{\alpha_{\mathrm{L}}}}\right)^{\frac{\alpha_{\mathrm{L}}}{\alpha_{\mathrm{N}}}}\right)\right]$. Define two convex functions $\varphi_1(u) = \exp(-u)$ and $\varphi_2(u) = \exp(-u^{\frac{\alpha_{\mathrm{L}}}{\alpha_{\mathrm{N}}}})$. Since we assume the BS is associated to the typical BS in this case, the CDF of the associated link path gain u becomes

$$F(u) = \exp\left(-\gamma_{\mathrm{T}}\lambda_{\mathrm{B}}u^{-\frac{1}{\alpha_{\mathrm{L}}}}\right). \tag{3.27}$$

By change of variables, we can obtain

$$\mathbb{E}_u\left[u^{-\frac{1}{\alpha_{\mathrm{L}}}}\right] = \frac{1}{\gamma_{\mathrm{T}}\lambda_{\mathrm{B}}}, \tag{3.28}$$

hence, by Jensen's inequality, the lower bound of $\mathcal{L}_{I_{\phi_{\mathrm{T}}}}(T,u)$ becomes

$$\mathcal{L}_{I_{\phi_{\mathrm{T}}}}(Tu^{-1}) \geq \mathcal{L}^{\mathrm{LB}}_{I_{\phi_{\mathrm{T}}}}(T,u) = \exp\left(-\frac{\beta_2}{\gamma_{\mathrm{T}}}\right) = \exp\left(-\varrho(T)\right). \tag{3.29}$$

Similarly, we have

$$\mathbb{E}_u\left[(\lambda_{\mathrm{B}}u^{-\frac{1}{\alpha_{\mathrm{L}}}})^{\frac{\alpha_{\mathrm{L}}}{\alpha_{\mathrm{N}}}}\right] = \left(\frac{1}{\gamma_{\mathrm{T}}}\right)^{\frac{\alpha_{\mathrm{L}}}{\alpha_{\mathrm{N}}}}\Gamma\left(1+\frac{\alpha_{\mathrm{L}}}{\alpha_{\mathrm{N}}}\right), \tag{3.30}$$

with the lower bound of $\mathcal{L}_{I_{\phi_{\mathrm{C}}}}(Tu^{-1})$ evaluated as

$$\mathcal{L}^{\mathrm{LB}}_{I_{\phi_{\mathrm{C}}}}(Tu^{-1}) = \exp\left(-\left(\frac{1}{\gamma_{\mathrm{T}}}\right)^{\frac{\alpha_{\mathrm{L}}}{\alpha_{\mathrm{N}}}}\beta_3\Gamma\left(1+\frac{\alpha_{\mathrm{L}}}{\alpha_{\mathrm{N}}}\right)\right)$$

$$= \exp\left(-2\lambda_{\mathrm{S}} c^{\frac{1}{\alpha_{\mathrm{N}}}} \Gamma\left(1-\frac{\alpha_{\mathrm{L}}}{\alpha_{\mathrm{N}}}\right) \Gamma\left(1+\frac{\alpha_{\mathrm{L}}}{\alpha_{\mathrm{N}}}\right) \varrho(T)^{\frac{\alpha_{\mathrm{L}}}{\alpha_{\mathrm{N}}}}\right). \tag{3.31}$$

Note that the argument inside (3.31) scales with λ_{S} and $c^{\frac{1}{\alpha_{\mathrm{N}}}}$, which makes the inside argument very small, therefore, it holds

$$\mathcal{L}^{\mathrm{LB}}_{I_{\phi_{\mathrm{T}}}}(Tu^{-1}) \ll \mathcal{L}^{\mathrm{LB}}_{I_{\phi_{\mathrm{C}}}}(Tu^{-1}) \approx 1. \tag{3.32}$$

From (3.31), it can be seen that the lower bound of LT of $I_{\phi_{\mathrm{C}}}$ scales exponentially with $\beta_3 = \gamma_{\mathrm{C}} \varrho(T)^{\frac{\alpha_{\mathrm{L}}}{\alpha_{\mathrm{N}}}}$, which further scales with $\lambda_{\mathrm{S}} c^{\frac{1}{\alpha_{\mathrm{N}}}}$. This leads to an intuitive insight that when the street intensity increases, the effects by cross BS interference grow larger. It should be noted from (3.32), that the cross BS interference is very small compared to typical BSs. And generally, the cross interference can be neglected, with a relatively large corner loss Δ.

Fig. 3.2 gives a comparison between the analytic and simulation results of the coverage probability when considering no interference (noise only), considering interference from only typical BSs, and both typical and cross BS interference, and all of the interference. It is shown that the coverage probabilities with and without the parallel BSs completely coincide. This verifies the corresponding proof in Proposition 2 that the parallel interference can be neglected. It can also be observed that the cross BS interference is also negligible compared to the typical BS interference, which is demonstrated in the Jensen's inequality lower bound analysis in (3.29) and (3.31). We set the corner loss in the simulation as $\Delta = 20$dB, and in this setting, we can conclude that under the Manhattan distance based pathloss model, the NLOS

interference (from cross/parallel BSs) is negligible. It will also be shown in Section 3.4 that with the corner loss ranging from 30dB to 0dB (no shadowing loss case), the coverage probability does not vary significantly. This indicates that whatever the corner loss is, the NLOS interference is always very small compared to the LOS interference.

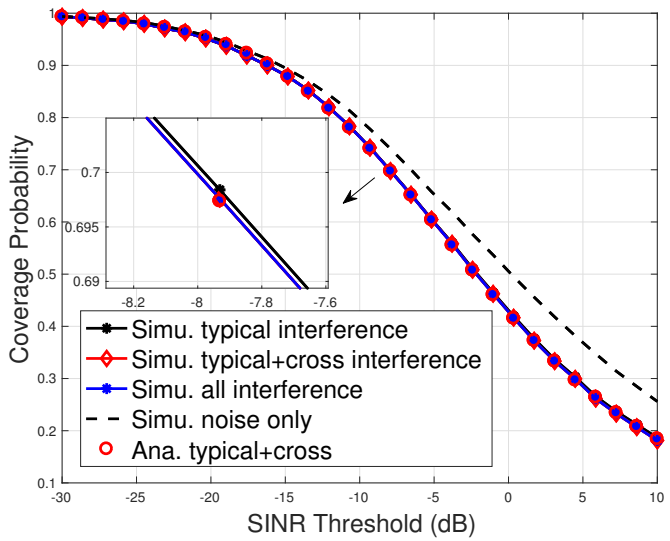

Figure 3.2: Comparison of the numerical and analytic coverage probability. The black/red/blue solid lines respectively represent the coverage probability considering only typical BS interference, both typical and cross BS interference and all interference. The black dashed line is the coverage probability simulated considering noise only. Red circles are the analytic expression of coverage probability in (3.21) – (3.26) considering interference from typical and cross BSs.

3.4 Scaling Laws with Network Densities

In this section, we analyze the scaling laws of the coverage probability and the association probability with the network densities, i.e., street intensity λ_{S} and BS intensity λ_{B}. We apply tight approximations to the relevant metrics and reveal interesting interplays of the performance with the network deployment.

3.4.1 Scaling laws with coverage probability

The coverage probability serves as an important metric in evaluating system performance, since it is closely related to ergodic rate and throughput outage. In this section, we focus on answering the following questions: i) how densely should BSs be deployed in urban streets to maximize coverage at a minimum cost? ii) how does the coverage probability change for different densities in different cities?

3.4.1.1 Scaling law with BS intensity

The interference limited scenario targets an asymptotic case, where the noise can be neglected and thus focus fully on the interplay between network intensities. This scenario can either be achieved by very high BS intensity or by very dense streets deployment.

Based on the coverage probability given in (3.21) and (3.22), after neglecting the noise term and changing variables by $x = \lambda_{\mathrm{B}} u^{-\frac{1}{\alpha_{\mathrm{L}}}}$, the expression

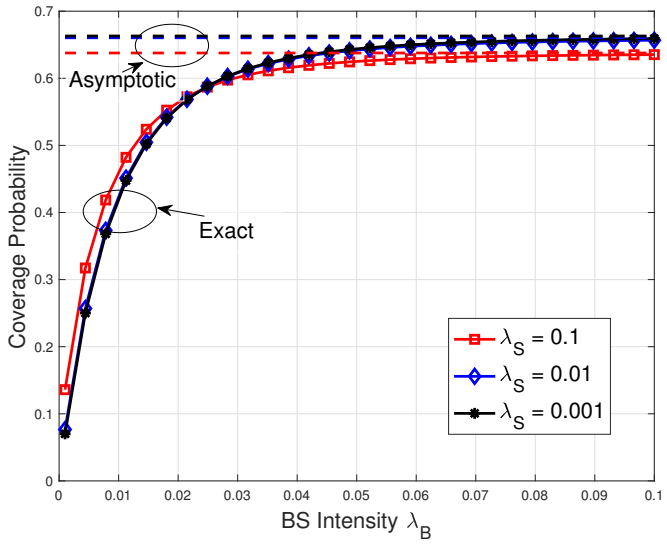

Figure 3.3: Asymptotic behavior of coverage probability with large BS intensity λ_{B}. Solid red, green and blue curves are respectively the coverage probability under different street intensities, $\lambda_{\mathrm{S}} = 0.1, 0.01$ and 0.001. Dashed curves represent the analytic asymptotic value of the coverage probability when BS intensity grows very large.

of the coverage probability becomes

$$P_{\mathrm{c}}(T) = \int_0^{\infty} \exp\left(-(\beta_2 + \gamma_{\mathrm{T}})x\right) \exp\left(-(\beta_3 + \gamma_{\mathrm{C}})x^{\frac{\alpha_{\mathrm{L}}}{\alpha_{\mathrm{N}}}}\right) \left(\gamma_{\mathrm{T}} + \frac{\gamma_{\mathrm{C}}\alpha_{\mathrm{L}}}{\alpha_{\mathrm{N}}} x^{\frac{\alpha_{\mathrm{L}}}{\alpha_{\mathrm{N}}}-1}\right) dx, \tag{3.33}$$

where β_2, β_3, γ_{T} and γ_{C} are provided in Section 3.

Under the modeling of BSs as PPPs and the Manhattan distance pathloss model, one interesting observation from (3.33) is that the coverage probability is independent of the BS intensity. On one hand, when both street and BSs intensities grow very large, it is intuitive that with ultra dense deployment of BSs, i.e., $\lambda_{\mathrm{B}} \to \infty$, both the associated path gain and interference become very large, and their effects on the coverage probability cancel out, which leads to

an asymptotic value of the coverage probability. On the other hand, when only the street intensity itself grows very large, the scenario could also be interference limited. In this case, the coverage probability is still a constant, however densely the BSs are deployed. This reveals an important insight that when street intensity grows large, the increase of coverage probability by deploying denser BSs is less significant. We plot Fig. 3.3 to demonstrate the above two observations in an ultra-dense network where intensity of BS grows very large. First, it is shown that from approximately $\lambda_{\mathrm{B}} = 0.05$ (BS spacing of 20m) for different street intensities, the coverage probability starts to converge to the asymptotic value. Second, with denser street distribution (e.g., $\lambda_{\mathrm{S}} = 0.1$, red curve), the increase of coverage probability is less prominent. Also, denser street distribution leads to lower asymptotic coverage probability.

3.4.1.2 Scaling law with street intensity

In the last section, we demonstrated the impact of different city streets (with different intensities) on the coverage probability enhancement. Next, we reveal the relationship between the coverage probability and the urban street intensity. One important thing to note is that in the dense street case, the street intensity λ_{s} is not arbitrarily large, where the most dense street might be at least 20m spacing, with $\lambda_{\mathrm{S}} = 0.05$. We provide the following proposition to quantify how the coverage probability changes under different street intensities and prove it herein.

Proposition 3. 1) When the BS intensity λ_{B} is large, the coverage probability

decreases linearly with the street intensity λ_{S}. 2) When λ_{B} is small, the coverage probability increases linearly with λ_{S}.

Proof. In terms of the linear scaling law and its dependence on the BS intensity, we provide the following steps of the proof:

Linear scaling law First, from (3.21) – (3.26), the coverage probability can be rewritten as

$$P_{\mathrm{c}}(T) = P_1 + P_2, \tag{3.34}$$

where

$$\begin{aligned} P_1 = &\int_0^{\infty} \exp\left(-\beta_1 u^{-1}\right) \exp\left(-(\beta_2+\gamma_{\mathrm{T}})\lambda_{\mathrm{B}} u^{-\frac{1}{\alpha_{\mathrm{L}}}}\right) \\ &\times \exp\left(-(\beta_3+\gamma_{\mathrm{C}})\lambda_{\mathrm{B}}^{\frac{\alpha_{\mathrm{L}}}{\alpha_{\mathrm{N}}}} u^{-\frac{1}{\alpha_{\mathrm{N}}}}\right)\left(\frac{\lambda_{\mathrm{B}}\gamma_{\mathrm{T}}}{\alpha_{\mathrm{L}}} u^{-\frac{1}{\alpha_{\mathrm{L}}}-1}\right) du, \end{aligned} \tag{3.35}$$

and

$$\begin{aligned} P_2 = &\int_0^{\infty} \exp\left(-\beta_1 u^{-1}\right) \exp\left(-(\beta_2+\gamma_{\mathrm{T}})\lambda_{\mathrm{B}} u^{-\frac{1}{\alpha_{\mathrm{L}}}}\right) \\ &\times \exp\left(-(\beta_3+\gamma_{\mathrm{C}})\lambda_{\mathrm{B}}^{\frac{\alpha_{\mathrm{L}}}{\alpha_{\mathrm{N}}}} u^{-\frac{1}{\alpha_{\mathrm{N}}}}\right)\left(\frac{\gamma_{\mathrm{C}}}{\alpha_{\mathrm{N}}}\lambda_{\mathrm{B}}^{\frac{\alpha_{\mathrm{L}}}{\alpha_{\mathrm{N}}}} u^{-\frac{1}{\alpha_{\mathrm{N}}}-1}\right) du. \end{aligned} \tag{3.36}$$

We then rewrite the second part in (3.36), by integration by parts, as

$$\begin{aligned} P_2 = &\frac{\gamma_{\mathrm{C}}}{\gamma_{\mathrm{C}}+\beta_3} \int_0^{\infty} \exp\left(-\beta_1 u^{-1}\right) \exp\left(-(\beta_2+\gamma_{\mathrm{T}})\lambda_{\mathrm{B}} u^{-\frac{1}{\alpha_{\mathrm{L}}}}\right) \\ &\times \frac{\partial\left[\exp\left(-(\beta_3+\gamma_{\mathrm{C}})\lambda_{\mathrm{B}}^{\frac{\alpha_{\mathrm{L}}}{\alpha_{\mathrm{N}}}} u^{-\frac{1}{\alpha_{\mathrm{N}}}}\right)\right]}{\partial u} \end{aligned}$$

$$= \frac{\gamma_{\mathrm{C}}}{\gamma_{\mathrm{C}}+\beta_3} - \frac{\gamma_{\mathrm{C}}}{\gamma_{\mathrm{C}}+\beta_3}\int_0^{\infty} \exp\left(-(\beta_3+\gamma_{\mathrm{C}})\lambda_{\mathrm{B}}^{\frac{\alpha_{\mathrm{L}}}{\alpha_{\mathrm{N}}}} u^{-\frac{1}{\alpha_{\mathrm{N}}}}\right)$$
$$\times \frac{\partial\left[\exp\left(-\beta_1 u^{-1}\right)\exp\left(-(\beta_2+\gamma_1)\lambda_{\mathrm{B}} u^{-\frac{1}{\alpha_{\mathrm{L}}}}\right)\right]}{\partial u}. \tag{3.37}$$

In both (3.37) and (3.35), only $\beta_3 = \zeta_1\lambda_{\mathrm{S}}$, and $\gamma_{\mathrm{C}} = \zeta_2\lambda_{\mathrm{S}}$ depend on λ_{S}. Further, β_3 scales linearly with γ_{C}, which itself is very small due to the terms λ_{S} and $c^{\frac{1}{\alpha_{\mathrm{N}}}}$. Then, by applying a first-order Taylor approximation $\exp(-x) \approx 1 - x$ to $\exp\left(-(\beta_3+\gamma_{\mathrm{C}})\lambda_{\mathrm{B}}^{\frac{\alpha_{\mathrm{L}}}{\alpha_{\mathrm{N}}}} u^{-\frac{1}{\alpha_{\mathrm{N}}}}\right) \approx 1-\lambda_{\mathrm{s}}(\zeta_1+\zeta_2)\lambda_{\mathrm{B}}^{\frac{\alpha_{\mathrm{L}}}{\alpha_{\mathrm{N}}}} u^{-\frac{1}{\alpha_{\mathrm{N}}}}$ in (3.35) and (3.37), we can see P_1 and P_2 scale linearly with λ_{S}, hence proving the linear scaling law of coverage probability with λ_{S}. Fig. 3.4 compares the exact coverage probability in (3.34) and that with Taylor approximation. It is shown that under different street intensities $\lambda_{\mathrm{S}} = 0.001, 0.01, 0.02$, the exact results match well with the Taylor approximations. This verifies the accuracy of using Taylor approximation to prove the linear scaling law. Another observation here is when the street density is relatively small, e.g., $\lambda_{\mathrm{S}} = 0.001$, the coverage probability is insensitive to the NLOS pathloss exponent α_{N}, since the coverage almost remains a constant with α_{N} ranging from 3 to 10. When streets become dense, the coverage probability decreases faster with growing α_{N}. This is consistent with the fact that α_{N} only affects pathloss of the NLOS links.

Dependence on BS intensity To demonstrate the different scaling laws of coverage probability with BS intensities, we take out the components in (3.33),

which are dependent on λ_{S} of the integral, and define it as $\Upsilon(\lambda_{\mathrm{S}})$, which is

$$\Upsilon(\lambda_{\mathrm{S}}) = \exp\left(-\lambda_{\mathrm{S}}\left(\zeta_1+\zeta_2\right)\lambda_{\mathrm{B}}^{\frac{\alpha_{\mathrm{L}}}{\alpha_{\mathrm{N}}}}u^{-\frac{1}{\alpha_{\mathrm{N}}}}\right)\left(\frac{\lambda_{\mathrm{B}}\gamma_{\mathrm{T}}}{\alpha_{\mathrm{L}}}u^{-\frac{1}{\alpha_{\mathrm{L}}}-1}+\frac{\lambda_{\mathrm{s}}\zeta_2\lambda_{\mathrm{B}}^{\frac{\alpha_{\mathrm{L}}}{\alpha_{\mathrm{N}}}}}{\alpha_{\mathrm{N}}}u^{-\frac{1}{\alpha_{\mathrm{N}}}-1}\right), \tag{3.38}$$

the derivative of which is

$$\begin{aligned}\Upsilon'(\lambda_{\mathrm{S}}) = &\frac{\lambda_{\mathrm{B}}^{\frac{\alpha_{\mathrm{L}}}{\alpha_{\mathrm{N}}}}}{\alpha_{\mathrm{N}}}u^{-\frac{1}{\alpha_{\mathrm{N}}}-1}\exp\left(-\lambda_{\mathrm{S}}\left(\zeta_1+\zeta_2\right)\lambda_{\mathrm{B}}^{\frac{\alpha_{\mathrm{L}}}{\alpha_{\mathrm{N}}}}u^{-\frac{1}{\alpha_{\mathrm{N}}}}\right)\\ &\times\left(\zeta_2-(\zeta_1+\zeta_2)\alpha_{\mathrm{N}}\left[\frac{\gamma_{\mathrm{T}}\lambda_{\mathrm{B}}}{\alpha_{\mathrm{L}}}u^{-\frac{1}{\alpha_{\mathrm{L}}}}+\frac{\lambda_{\mathrm{S}}\zeta_2\lambda_{\mathrm{B}}^{\frac{\alpha_{\mathrm{L}}}{\alpha_{\mathrm{N}}}}}{\alpha_{\mathrm{N}}}u^{-\frac{1}{\alpha_{\mathrm{N}}}}\right]\right).\end{aligned} \tag{3.39}$$

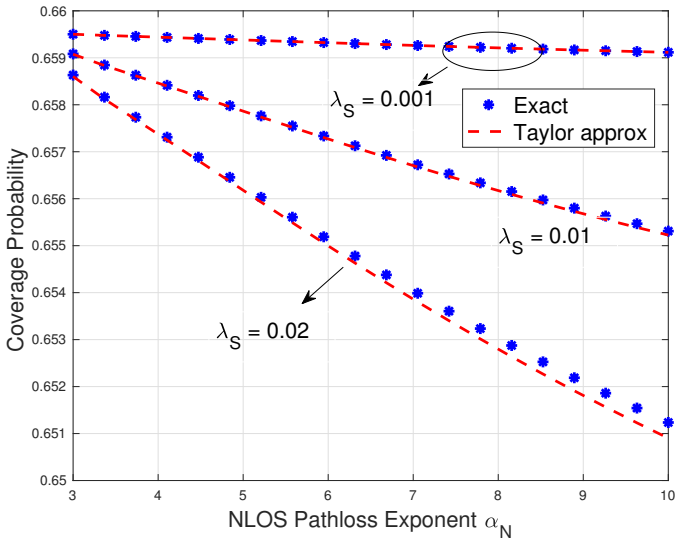

Figure 3.4: Comparison of the exact and Taylor approximation of coverage probability. Solid blue curves plot exact coverage probability in Theorem 3.3.1 under different street intensities, i.e., $\lambda_{\mathrm{S}} = 0.02, 0.01$ and 0.001. The blue stars are the exact coverage probability and the red dashed curves are the Taylor approximations to (3.35) and (3.37).

Since the exponential part from (3.39) is always positive, and ζ_2 and ζ_1 are independent of λ_{B}, it is clear that there exists a threshold λ_{B}^*, satisfying

$$\frac{\gamma_{\mathrm{T}}\lambda_{\mathrm{B}}^*}{\alpha_{\mathrm{L}}}u^{-\frac{1}{\alpha_{\mathrm{L}}}} + \frac{\lambda_{\mathrm{S}}\zeta_2{\lambda_{\mathrm{B}}^*}^{\frac{\alpha_{\mathrm{L}}}{\alpha_{\mathrm{N}}}}}{\alpha_{\mathrm{N}}}u^{-\frac{1}{\alpha_{\mathrm{N}}}} = \frac{\zeta_2}{(\zeta_1+\zeta_2)\alpha_{\mathrm{N}}}. \tag{3.40}$$

Hence, when $\lambda_{\mathrm{B}} > \lambda_{\mathrm{B}}^*$, $\Upsilon'(\lambda_{\mathrm{S}}) < 0$, which indicates when intensity of BSs grows large, coverage probability decreases with λ_{S}. Also, when $\lambda_{\mathrm{B}} < \lambda_{\mathrm{B}}^*$, denser streets lead to higher coverage probability. □

Fig. 3.5 illustrates the linear scaling of the coverage probability with the intensity of streets λ_{S}. It first can be observed that the coverage probability scales linearly with the intensity of streets, and the coverage probability increases with λ_{S} while decreases with corner loss Δ, when the BS intensity is relatively small $\lambda_{\mathrm{B}} = 0.01$. Also, the coverage probability decreases with λ_{S} with large BS intensity $\lambda_{\mathrm{B}} = 0.1$, while it increases with corner loss in the meantime. This implies that when the BS deployment is dense, interference becomes dominant and larger corner loss reduces the interference; when BSs are relatively sparse, small corner loss strengthens the signal from the cross BSs, thus making the associated link received power stronger and enhancing the coverage probability. Also, it can be observed that when the corner loss becomes small (e.g., the no shadowing loss case $\Delta = 0$dB), the coverage probability becomes more sensitive to the change of street intensities, which is shown by a larger slope of the curve of coverage probability. This is because the smaller corner loss makes the cross BS interference more prominent, thus increasing the sensitivity of coverage probability to the street intensities.

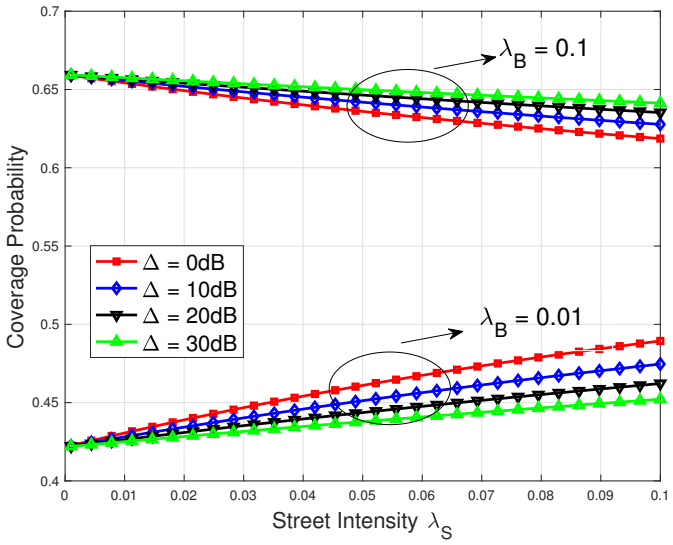

Figure 3.5: Scaling of coverage probability with different street intensity λ_S. Comparison is made between sparse/dense BS intensities $\lambda_B = 0.01, 0.1$ and different corner losses, considering no corner shadowing loss and very severe corner loss cases $\Delta = 0, 10, 20, 30$dB.

It is clear from Section 3.4.1.2 that the microcellular network does not work efficiently in a scenario where both BS and street intensities are very large. When the BSs are very sparse on each street, increased street intensity makes it more likely to be associated with a BS on cross streets, thus leading to a larger associated path gain. When λ_B grows large, however, the system becomes interference-limited, thus denser streets only contribute to more interference and lower the coverage probability. This sheds light on how to deploy BSs more efficiently under different street intensities. Specifically, when the streets are very dense, relatively sparse BSs should be deployed since coverage probability increases more slowly with more BSs; when the streets are

sparse, we could deploy denser BSs to enhance coverage probability (however, too many BSs are inefficient due to the asymptotic behavior of coverage in ultra-dense network).

3.4.2 Scaling law with BS association

In this section, we analyze the BS association under the Manhattan distance based pathloss model in MPLP. We start with the analysis of association probability. Given the CDF of the associated link path gain in Section 3.2, we derive the probability the receiver is associated with a LOS BS on the typical street.

Corollary 3.4.0.1. *The probability χ_{T} that the receiver is associated with a typical BS is*

$$\begin{aligned}\chi_{\mathrm{T}} &\overset{(a)}{=} \mathbb{E}_u\left\{\mathbb{P}\left(u_{\mathrm{C}} < u \middle| u_{\mathrm{T}} = u\right)\right\} = \mathbb{E}_{u_{\mathrm{T}}}\left\{\mathbb{P}\left(u_{\mathrm{C}} < u_{\mathrm{T}}\right)\right\} \\ &\overset{(b)}{=} \int_0^{\infty} \exp\left(-\gamma_{\mathrm{C}}\lambda_{\mathrm{B}}^{\frac{\alpha_{\mathrm{L}}}{\alpha_{\mathrm{N}}}} u^{-\frac{1}{\alpha_{\mathrm{N}}}} - \gamma_{\mathrm{T}}\lambda_{\mathrm{B}} u^{-\frac{1}{\alpha_{\mathrm{L}}}}\right) \frac{\gamma_{\mathrm{T}}\lambda_{\mathrm{B}}}{\alpha_{\mathrm{L}}} u^{-\frac{1}{\alpha_{\mathrm{L}}}-1} du \\ &\overset{(c)}{=} \gamma_{\mathrm{T}} \int_0^{\infty} \exp\left(-\gamma_{\mathrm{C}} x^{\frac{\alpha_{\mathrm{L}}}{\alpha_{\mathrm{N}}}} - \gamma_{\mathrm{T}} x\right) dx, \end{aligned} \tag{3.41}$$

where (a) is conditioned of maximum path gain of typical BSs is u, (b) is based on the CDF of the maximum path gain of typical/cross BSs, (c) follows by change of variables $x = \lambda_{\mathrm{B}} u^{-\frac{1}{\alpha_{\mathrm{L}}}}$.

Since the argument of the second exponential function in (3.41) is the multiplication of λ_{S} and an additional attenuation of corner loss, the argument inside tends to be very small. Similar to the approximation in Section 3.4, we

approximate the association probability by

$$\chi_{\mathrm{T}}^{\mathrm{Approx}} = \int_0^{\infty} \exp\left(-\mu\right) \left(1 - \frac{\zeta_2}{\gamma_{\mathrm{T}}^{\frac{\alpha_{\mathrm{L}}}{\alpha_{\mathrm{N}}}}} \lambda_{\mathrm{S}} \mu^{\frac{\alpha_{\mathrm{L}}}{\alpha_{\mathrm{N}}}}\right) d\mu$$
$$= 1 - \frac{2^{\frac{\alpha_{\mathrm{L}}}{\alpha_{\mathrm{N}}}+1} \gamma_{\mathrm{C}}}{\gamma_{\mathrm{T}}^{\frac{\alpha_{\mathrm{L}}}{\alpha_{\mathrm{N}}}}} \left[\mathrm{sinc}\left(\frac{\alpha_{\mathrm{L}}}{\alpha_{\mathrm{N}}}\right)\right]^{-1} \lambda_{\mathrm{S}}, \tag{3.42}$$

where $\mathrm{sinc}(x) = \frac{\sin \pi x}{\pi x}$. Because the sinc function monotonously decreases with x $(0 < x < 1)$, the association probability with a typical BS decreases with α_{L}. Fig. 3.6 shows the comparison of the exact association probability in (3.41) and the approximation results in (3.42). The approximation in (3.42) is tight when there exists corner loss $\Delta = 20\mathrm{dB}$, while the gap increases in the no shadowing case. There exists a linear scaling law for the association probability with the street intensity in the scenarios with significant shadowing loss at corner, which is shown in Fig. 3.6. Different from α_{N} which only impacts on the NLOS BS pathloss, the LOS pathloss exponent α_{L} is involved in both the calculation of typical/cross BS pathloss. The decrease of LOS association probability with larger α_{L} implies that the LOS link pathloss is more sensitive to the changing pathloss exponents. Also, it is intuitive that the increase of α_{N} enhances the association probability since it further attenuates the transmit signal from cross street BSs. It should be noted that it is meaningful to examine the interplay between the coverage probability and these exponents values, since the pathloss exponent in reality is not fixed (we extract two reasonable parameters for the ease of analysis in this thesis), but is a random variable varying from streets to streets [26]. The interplay of pathloss exponents and

LOS probability sheds light on the different BS association behaviors on different streets in an urban area.

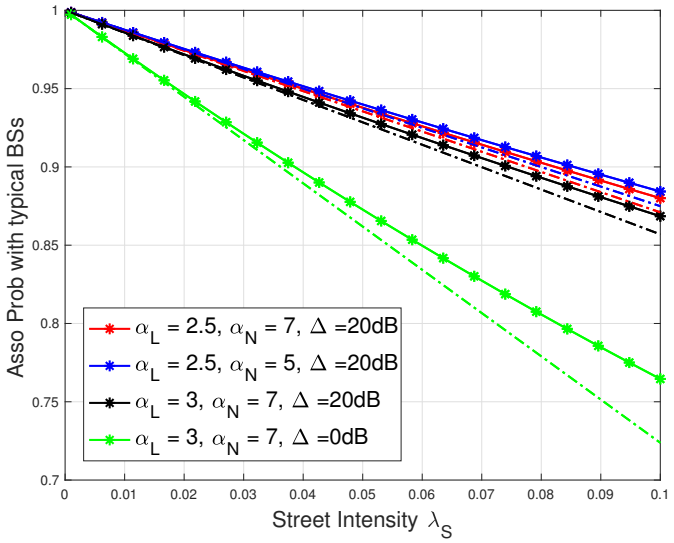

Figure 3.6: Illustration of the association probability with an optically LOS BS. The solid lines represent the simulation result and the dashed lines are the approximations in (3.42).

In addition, from (3.42) there is a linear scaling law of LOS association probability with the intensity of cross streets in Fig. 3.6. Also, it should be noted that with the corner shadowing loss, even in an extremely dense street network, e.g., $\lambda_S = 0.1$, the association probability with typical BSs χ_T is still greater than 0.8. Only when in the case with no shadowing loss, the association probability χ_T decreases significantly the street intensity λ_S. The above association probability analysis illuminates another important observation that considering shadowing loss at a reasonable value, cross BSs play a very minor role in BS association under the Manhattan distance based mi-

crocellular pathloss model. Similar effects on coverage probability have been demonstrated in Section 3.3.

Hence, we can make the following conclusions about the BS association. First, the BS association probability is independent of the BS intensities. Second, the association probability decreases linearly with the intensity of the cross streets. Also, LOS association is less likely when the LOS pathloss exponent α_{L} increases.

Chapter 4

Comparison of Different Street Models

In this section, we compare the ergodic rate under three different street models. The MPLP street modeling in this thesis, fixed grid model (fixed spacing between streets) and realistic street deployments in Chicago. The raw street data is obtained *OpenStreetMap* powered by open source software and

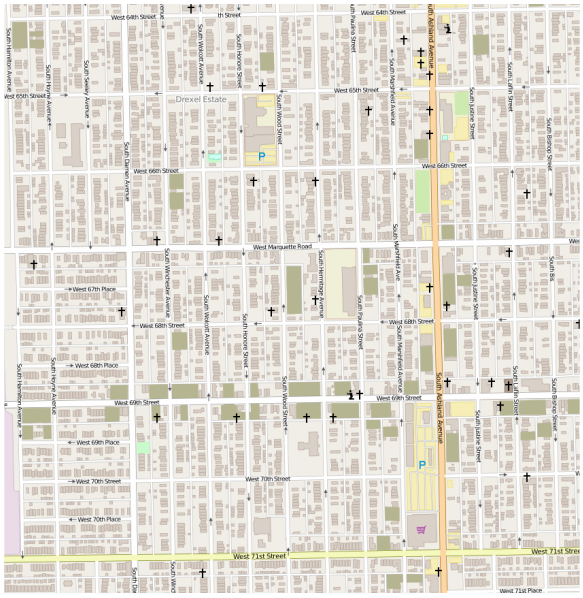

Figure 4.1: A snapshot of part of Chicago area from OpenStreetMap (Latitude: 41.762N - 41.78N, Longitude: -87.678W →- 87.658W), with a size of 1.659×2.002 (km^2).

[29], [**?**]. The simulated area is a part of Chicago given in Fig. 4.1, and map

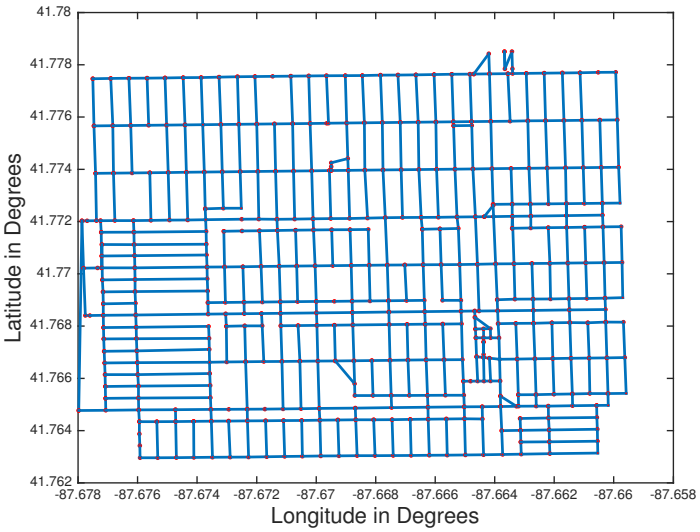

Figure 4.2: Streets abstracted from OpenStreetMap by QGIS. The red points are the intersections obtained from QGIS and the plot is obtained by lining up the intersections that has one common intersected street.

exported to Matlab is plotted in Fig. 4.2.

The comparison of the ergodic rate under the three models is given in Fig. 5.1. From this figure, it is clear that the capacities are very close under these different street models, which nearly coincide. Also, compared to the fixed grid model, which is widely adopted in Manhattan-kind urban street modeling, the MPLP model has the merit of yielding fairly tractable analysis. Its accuracy and tractability hence make MPLP a strong candidate in modeling urban street networks.

Chapter 5

Conclusion

In this thesis, we proposed a mathematical framework to model a Manhattan-type microcellular network under the urban mmWave communication system by stochastic geometry. We first analyze the distribution of the path gain to the BS. We then derive an exact yet concise expression of the coverage probability. The LOS interference from the BSs on the same street as the serving BS is the dominating factor in determining the coverage probability, while BSs on cross and parallel streets have insignificant effects. It was shown that in the ultra-dense network where intensity of BSs grows large,

the network is interference-limited and the coverage probability approaches an asymptotic value. Also, the coverage probability scales linearly with the intensity of streets, and displays an interesting interplay with the BS intensity: i) when BS deployment is dense, coverage probability decreases with street intensity; ii) when BS intensity is small, the coverage probability increases with street intensity. This implies that the system does not work efficiently when both BS and street intensities are very large. Therefore, there is no need to deploy many BSs in an already dense urban street environment. In addition, we showed that the LOS BSs still dominate the performance of the

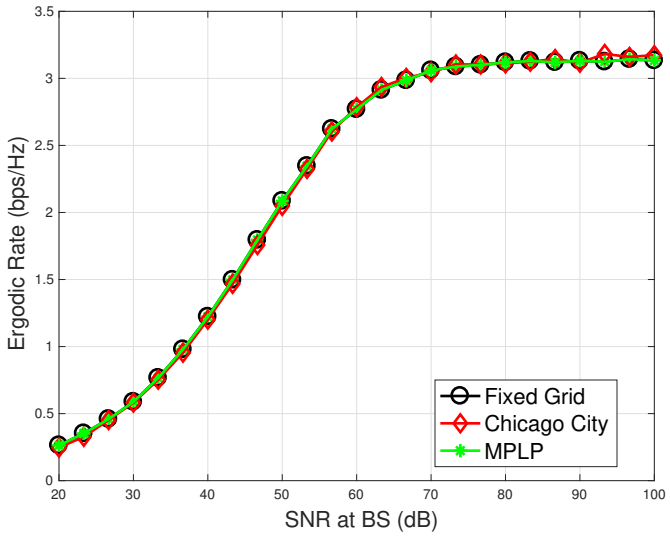

Figure 5.1: Comparison of ergodic rate among MPLP street modeling, fixed grid model and real streets obtained from Chicago city.

whole system, from the perspective of both BS association, as well as coverage. Also, it was shown that the probability that a receiver associates to LOS BSs is independent of the intensity of BSs, while it decreases linearly with the intensity of streets. Further, the LOS link is more sensitive to the change of propagation environments, i.e., the change of LOS pathloss exponent. Finally, we numerically compared the ergodic rates under MPLP, fixed spacing and a realistic Chicago street model. It was shown that the ergodic rate under these street models match well, reinforcing the validity of MPLP as a realistic yet accurate urban street model.

Bibliography

[1] Jeffrey Miller. Vehicle-to-vehicle-to-infrastructure (V2V2I) intelligent transportation system architecture. In *Proc. Intelligent Vehicles Symposium*, pages 715–720. IEEE, 2008.

[2] Pavle Belanovic, Danilo Valerio, Alexander Paier, Thomas Zemen, Fabio Ricciato, and Christoph F Mecklenbrauker. On wireless links for vehicle-to-infrastructure communications. *IEEE Trans. Veh. Technol.*, 59(1):269–282, 2010.

[3] J. Gozalvez, M. Sepulcre, and R. Bauza. IEEE 802.11p vehicle to infrastructure communications in urban environments. *IEEE Commun. Mag.*, 50(5):176–183, May 2012.

[4] Zhouyue Pi and Farooq Khan. An introduction to millimeter-wave mobile broadband systems. *IEEE Commun. Mag.*, 49(6):101–107, 2011.

[5] Theodore S Rappaport, Shu Sun, Rimma Mayzus, Hang Zhao, Yaniv Azar, Kevin Wang, George N Wong, Jocelyn K Schulz, Mathew Samimi, and Felix Gutierrez. Millimeter wave mobile communications for 5G cellular: It will work! *IEEE access*, 1:335–349, 2013.

[6] Theodore S Rappaport, Robert W Heath Jr, Robert C Daniels, and

James N Murdock. *Millimeter wave wireless communications*. Pearson Education, 2014.

[7] Junil Choi, Nuria Gonzalez-Prelcic, Robert Daniels, Chandra R Bhat, and Robert W Heath Jr. Millimeter wave vehicular communication to support massive automotive sensing. *arXiv preprint arXiv:1602.06456*, 2016.

[8] Ho Ting Cheng, Hangguan Shan, and Weihua Zhuang. Infotainment and road safety service support in vehicular networking: From a communication perspective. *Mechanical Systems and Signal Processing*, 25(6):2020–2038, 2011.

[9] A. V. Alejos, M. G. Sanchez, and I. Cuinas. Measurement and analysis of propagation mechanisms at 40 GHz: Viability of site shielding forced by obstacles. *IEEE Trans. Veh. Technol.*, 57(6):3369–3380, Nov 2008.

[10] Vutha Va, Takayuki Shimizu, Gaurav Bansal, and Robert W Heath Jr. Millimeter wave vehicular communications: A survey. *Foundations and Trends® in Networking*, 10(1), 2016.

[11] Young Niu, Youg Li, Depeng Jin, Li Su, and Athanasios V Vasilakos. A survey of millimeter wave (mmWave) communications for 5G: Opportunities and challenges. *arxiv. org*, pages 1–17, 2015.

[12] Jeffrey G Andrews, François Baccelli, and Radha Krishna Ganti. A tractable approach to coverage and rate in cellular networks. *IEEE Trans.*

Commun., 59(11):3122–3134, 2011.

[13] Tianyang Bai and Robert W Heath. Coverage and rate analysis for millimeter-wave cellular networks. *IEEE Trans. Wireless Commun.*, 14(2):1100–1114, 2015.

[14] François Baccelli and Xinchen Zhang. A correlated shadowing model for urban wireless networks. In *Proc. IEEE Infocom.*, pages 801–809. IEEE, 2015.

[15] Jeffrey G Andrews, Tianyang Bai, Mandar Kulkarni, Ahmed Alkhateeb, Abhishek Gupta, and Robert W Heath. Modeling and analyzing millimeter wave cellular systems. *IEEE Trans. Commun.*, 2016.

[16] Hisham Elshaer, Mandar N Kulkarni, Federico Boccardi, Jeffrey G Andrews, and Mischa Dohler. Downlink and uplink cell association with traditional macrocells and millimeter wave small cells. *IEEE Trans. Wireless Commun.*, 15(9):6244–6258, 2016.

[17] Marco Di Renzo. Stochastic geometry modeling and analysis of multitier millimeter wave cellular networks. *IEEE Trans. Wireless Commun.*, 14(9):5038–5057, 2015.

[18] Tianyang Bai, Rahul Vaze, and Robert W Heath. Analysis of blockage effects on urban cellular networks. *IEEE Trans. Wireless Commun.*, 13(9):5070–5083, 2014.

[19] Mandar N Kulkarni, Sarabjot Singh, and Jeffrey G Andrews. Coverage and rate trends in dense urban mmwave cellular networks. In *IEEE GLOBECOM*, pages 3809–3814. IEEE, 2014.

[20] J. Lee, X. Zhang, and F. Baccelli. A 3-D spatial model for in-building wireless networks with correlated shadowing. *IEEE Trans. Wireless Commun.*, 15(11):7778–7793, Nov 2016.

[21] Andreas F Molisch, Aki Karttunen, Rui Wang, C Umit Bas, Sooyoung Hur, Jeongho Park, and Jianzhong Zhang. Millimeter-wave channels in urban environments. In *Proc. 10th European Conference on Antennas and Propagation (EuCAP)*, pages 1–5. IEEE, 2016.

[22] George R MacCartney, Junhong Zhang, Shuai Nie, and Theodore S Rappaport. Path loss models for 5g millimeter wave propagation channels in urban microcells. In *Global Communications Conference (GLOBECOM), 2013 IEEE*, pages 3948–3953. IEEE, 2013.

[23] Theodore S Rappaport, Felix Gutierrez, Eyal Ben-Dor, James N Murdock, Yijun Qiao, and Jonathan I Tamir. Broadband millimeter-wave propagation measurements and models using adaptive-beam antennas for outdoor urban cellular communications. *IEEE Trans. Antennas and Propogation*, 61(4):1850–1859, 2013.

[24] V Nurmela, A Karttunen, A Roivainen, L Raschkowski, T Imai, J Jarvelainen, J Medbo, J Vihriala, J Meinila, K Haneda, et al. Metis channel models. *FP7 METIS, Deliverable D*, 1, 2015.

[25] Katsuyuki Haneda, Lei Tian, Yi Zheng, Henrik Asplund, Jian Li, Yi Wang, David Steer, Clara Li, Tommaso Balercia, Sunguk Lee, et al. 5G 3GPP-like channel models for outdoor urban microcellular and macrocellular environments. *arXiv preprint arXiv:1602.07533*, 2016.

[26] Andreas F. Molisch, Aki Karttunen, Sooyoung Hur, Jeongho Park, and Jianzhong Zhang. Spatially consistent pathloss modeling for millimeter-wave channels in urban environments. In *Proc. 10th European Conference on Antennas and Propagation (EuCAP)*, pages 1–5, 2016.

[27] Y. Wang, Kiran. Venugopal, Andreas. F. Molisch, and Robert W. Heath Jr. Analysis of urban millimeter wave microcellular networks. In *Proc. IEEE VTC fall*, pages 1–5, Sept. 2016.

[28] K. Venugopal, M. C. Valenti, and R. W. Heath. Device-to-device millimeter wave communications: Interference, coverage, rate, and finite topologies. *IEEE Trans. Wireless Commun.*, 15(9):6175–6188, Sept 2016.

[29] `http://www.openstreetmap.org/`,.

[30] Mordechai Haklay and Patrick Weber. Openstreetmap: User-generated street maps. *IEEE Pervasive Computing*, 7(4):12–18, 2008.

[31] Frederik Ramm, Jochen Topf, and Steve Chilton. *OpenStreetMap: using and enhancing the free map of the world*. UIT Cambridge Cambridge, 2011.

[32] DT QGIS. Quantum GIS geographic information system. *Open Source Geospatial Foundation Project*, 45, 2011.

[33] François Baccelli and Bartlomiej Blaszczyszyn. *Stochastic geometry and wireless networks: Theory*, volume 1. Now Publishers Inc, 2009.

[34] Sung Nok Chiu, Dietrich Stoyan, Wilfrid S Kendall, and Joseph Mecke. *Stochastic geometry and its applications*. John Wiley & Sons, 2013.

[35] Salam Akoum, Omar El Ayach, and Robert W Heath. Coverage and capacity in mmwave cellular systems. In *IEEE Asilomar*, pages 688–692. IEEE, 2012.

[36] J. E. Berg. A recursive method for street microcell path loss calculations. In *Proc. PIMRC*, volume 1, pages 140–143 vol.1, Sep 1995.

[37] Izrail Solomonovich Gradshteyn and Iosif Moiseevich Ryzhik. *Table of integrals, series, and products*. Academic press, 2014.

[38] `http://dlmf.nist.gov/10.30#SS1.info`,.

Vita

Yuyang Wang is a graduate student at The University of Texas at Austin. She completed her B.S. in Electrical Engineering from Southeast University, Nanjing, China, in 2015. Her research interests lie in the broad area of mmWave communications and "connected vehicles". She is particularly interested in the modeling and design of safety applications by vehicle-to-infrastructure systems, and the values brought by wireless infrastructures in avoiding potential collisions and promoting driver safety under different automation levels.

Permanent address: 7630 Wood Hollow Dr.
Austin, Texas 78731

This thesis was typeset with LaTeX[†] by the author.

[†]LaTeX is a document preparation system developed by Leslie Lamport as a special version of Donald Knuth's TeX Program.